Inorganic Chemistry

pubs.acs.org/IC Article

Antitumor Effects of Ir(III)-2*H*-Indazole Complexes for Triple Negative Breast Cancer

Rajeeva Lochana Panchangam, Ramdas Nishanth Rao, Musuvathi Motilal Balamurali, Tejashri B. Hingamire, Dhanasekaran Shanmugam, Venkatraman Manickam, and Kaushik Chanda*

Cite This: *Inorg. Chem.* 2021, 60, 17593−17607 Read Online

ACCESS | Metrics & More | Article Recommendations | Supporting Information

ABSTRACT: In this work, we have synthesized a series of novel C,N-cyclometalated 2*H*-indazole-ruthenium(II) and -iridium(III) complexes with varying substituents (H, CH_3, isopropyl, and CF_3) in the R_4 position of the phenyl ring of the 2*H*-indazole chelating ligand. All of the complexes were characterized by ^1H, ^{13}C, high-resolution mass spectrometry, and elemental analysis. The methyl-substituted 2*H*-indazole-Ir(III) complex was further characterized by single-crystal X-ray analysis. The cytotoxic activity of new ruthenium(II) and iridium(III) compounds has been evaluated in a panel of triple negative breast cancer (TNBC) cell lines (MDA-MB-231 and MDA-MB-468) and colon cancer cell line HCT-116 to investigate their structure−activity relationships. Most of these new complexes have shown appreciable activity, comparable to or significantly better than that of cisplatin in TNBC cell lines. R_4 substitution of the phenyl ring of the 2*H*-indazole ligand with methyl and isopropyl substituents showed increased potency in ruthenium(II) and iridium(III) complexes compared to that of their parent compounds in all cell lines. These novel transition metal-based complexes exhibited high specificity toward cancer cells by inducing alterations in the metabolism and proliferation of cancer cells. In general, iridium complexes are more active than the corresponding ruthenium complexes. The new Ir(III)-2*H*-indazole complex with an isopropyl substituent induced mitochondrial damage by generating large amounts of reactive oxygen species (ROS), which triggered mitochondrion-mediated apoptosis in TNBC cell line MDA-MB-468. Moreover, this complex also induced G2/M phase cell cycle arrest and inhibited cellular migration of TNBC cells. Our findings reveal the key roles of the novel C−N-cyclometalated 2*H*-indazole-Ir(III) complex to specifically induce toxicity in cancer cell lines through contributing effects of ROS-induced mitochondrial disruption along with chromosomal and mitochondrial DNA target inhibition.

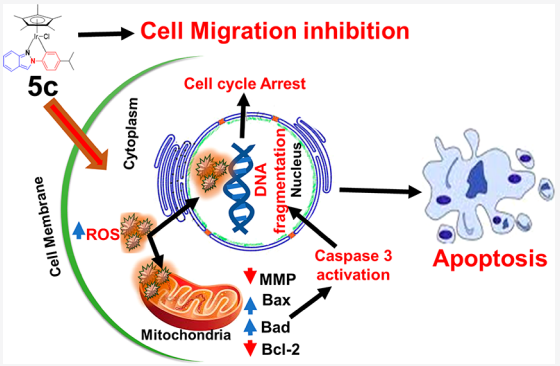

1. INTRODUCTION

The discovery of cisplatin as an anticancer drug by Rosenberg et al. in 1969 revolutionized cancer chemotherapy and extended the range of commonly applied chemotherapeutics purely from organic drugs to cyclometalated drugs.[1,2] Gandin et al. demonstrated the anticancer potential of the Pt(IV) derivative of cisplatin, with two axial ligands such as aspirin, ibuprofen, or dichloroacetate, or phenylbutyrate against human cancer cell lines with 100-fold more potency than cisplatin.[3] This further inspired medicinal chemists to look beyond for other possible and alternate chemotherapeutics that included metal complexes with Ru, Os, Ir, Fe, and Rh metal centers[4−8] specifically to overcome the limitations associated with platinum chemotherapy.[9] The design of cyclometalated half-sandwich metal complexes was based on the ability of hydrophobic arene ligands to facilitate free diffusion through the cell membrane along with additional coordinating sites for bidentate ligands, thus allowing the biological and pharmacological activities to be effectively tuned. Breast cancer is the world's second most common lethal cancer for women after lung cancer.[10] In the most prevalent triple negative breast cancer (TNBC), the cells do not express estrogen receptor (ER), progesterone receptor (PR), or human epidermal growth factor receptor 2 (HER-2), which are generally present in other therapeutically responsive breast cancer subtypes.[11] Moreover, the developed drug resistance caused by impaired hormonal HER-2 targeted therapy makes it very difficult to treat. For these reasons, though only 15−20% of breast cancers are of the TNBC type, it is considered as the most aggressive and highly metastatic and has a poor prognosis with increased risk of reoccurrence and low survival rates. However, chemotherapy remains a key therapeutic option for treating early and advanced stages of TNBC. Women with TNBC are

Received: July 21, 2021
Published: November 12, 2021

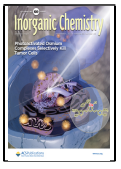

https://doi.org/10.1021/acs.inorgchem.1c02193
Inorg. Chem. 2021, 60, 17593−17607

reported to harbor mutations in the *BRCA* gene, which makes possible therapeutics that specifically inhibit DNA targets,[12,13] as evidenced with platinum complexes like cisplatin and carboplatin that are known to directly inhibit DNA. On the contrary, the development of severe side effects and drug resistance in TNBC patients made these compounds inefficient treatment options that paved the way for the development of other metal-based chemotherapeutics. Furthermore, this led to the development of the *in vivo* antimetastatic activity of ruthenium complexes[14,15] and less toxic ruthenium(II) and iridium(III)[16] complexes as angiogenesis inhibitors with their selective cytotoxicity. Cyclometalated Ir(III) complexes have been extensively studied for their anticancer activities, contrast-enhancing applications in cell imaging, and peptide labeling.[17] Recently, Komarnicka et al. studied the anticancer potential of half-sandwich Ir(III) complexes with phosphine derivatives of fluoroquinolones along with interaction among DNA, albumin, and apo-transferrin.[18] Targeting apoptosis, in particular mitochondrial targets (mutations that hamper its metabolism),[19] will be the primary aim in developing any anticancerous therapeutic strategies. Other possibilities for tuning mitochondrial functions include ceasing cancer cell proliferation and inducing cell death.[20,21] The recently developed mitochondrion-targeting chemotherapeutic molecules serve as promising candidates for targeting cancer cells.[22] Likewise, the novel synthesis and use of small heterocyclic molecules as potential chelating ligands for cyclometalation have also been well recognized in recent years. The currently prevalent rational design approaches serve as a tool for the generation of promising metallodrugs with improved anticancer activity.[23] The design concept for the currently synthesized 2*H*-indazole-bearing Ru and Ir complexes originated from the recognition of the biological role of the core 2*H*-indazole moiety in having antitumor[24] and modulatory activity versus estrogen receptors[25] and in theranostic applications.[26] Interestingly, the 2*H*-indazole ligands form the core in many best selling drugs such as pazopanib and niraparib, having the ability to target drug resistant, epidermal growth factor receptor (EGFR)-overexpressing tumors.[27]

Here we have designed the 2*H*-indazole C,N-cyclometalated ruthenium(II) and iridium(III) complexes with the hypothesis that altering substituents on the metal-coordinated ligands can influence the activity of the complex. Therefore, the phenyl ring of the ligand is substituted with both electron-donating and electron-withdrawing groups that favor the structure−activity relationship (SAR) of the complexes. In this work, we have investigated the cytotoxicity, apoptosis, cell cycle arrest, and inhibition of cell migration in a panel of triple negative breast cancer cell lines. We further demonstrate that these new complexes represent promising therapeutic agents for modulating triple negative breast cancer and could serve as an efficient strategy for modifying the existing metallo-drug cisplatin.

2. RESULTS AND DISCUSSION

2.1. Synthesis and Characterization of the Novel C−N Cyclometalated Complexes. The substituted 2*H*-indazole ligands **1** were synthesized via a one-pot synthetic transformation using Cu_2O rhombic dodecahedra as the nanocatalyst.[24] The ligands were substituted with electron-donating moieties (methyl, isopropyl, etc.) and a trifluoromethyl group as the electron-withdrawing moiety. All ligands reported here were synthesized by a cyclo-condensation reaction with an overall yield of 78−95%. Inspired by the introduction of C,N-cyclometalated complexes with heterocyclic ligands,[28] we attempted further synthesis of new cyclometalated 2*H*-indazole ruthenium(II) and iridium(III) complexes as depicted in Scheme 1, as anticancer agents on aggressive triple negative breast cancer cells.

Scheme 1. Synthesis of 2*H*-Indazole-Containing Ruthenium(II) and Iridium(III) Complexes

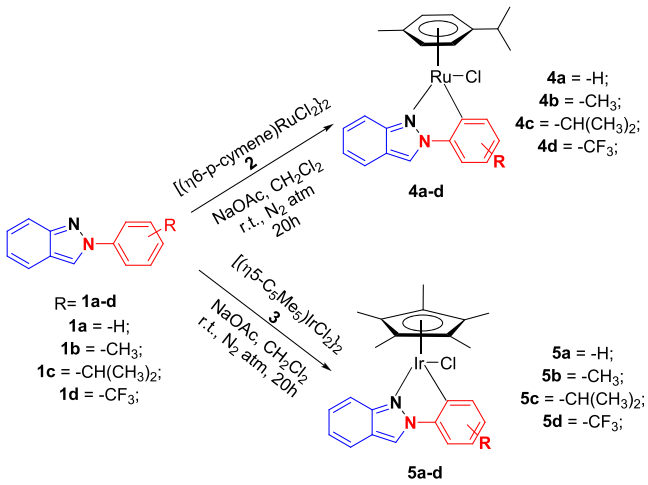

For the synthesis of ruthenium complexes **4a−d**, 2*H*-indazole ligands **1a−d** were treated with *p*-cymene ruthenium(II) $[(p\text{-cymene})RuCl_2]_2$ and sodium acetate in dichloromethane at room temperature under a N_2 atmosphere for 20 h to afford the corresponding complexes in 70−75% yields. Similarly, iridium complexes **5a−d** were synthesized using a similar method starting from the corresponding $[(\eta^5\text{-}C_5Me_5)\text{-}IrCl_2]_2$ in 80−85% yields. Structures of ruthenium complexes **4a−d** were unequivocally confirmed from the ^{1}H NMR spectra by the disappearance of one aromatic proton and the introduction of four doublets at 5.1−5.9 ppm, where as for half-sandwich iridium(III) complexes **5a−d**, the appearance of a singlet at 1.7 ppm for 15 protons corresponding to pentamethylcyclopentadienyl (C_5Me_5) moiety in ^{1}H NMR spectra confirmed the complexes. The structures of other synthesized complexes were also established by spectroscopic and analytical methods, including ^{1}H NMR, ^{13}C NMR, and ESI-MS techniques (Supporting Information). Compound **5b** was also characterized by X-ray diffraction from the crystal obtained by slow diffusion of hexane into a saturated solution of **5b** in CH_2Cl_2/EA. The structure and numbering are shown in Figure 1. Crystallographic data along with selected bond lengths and angles are listed in Tables S3−S9. The pentamethylcyclopentadienyl group displays the common π-bonded η^5-coordination mode, whereas the 2-(*p*-tolyl)-2*H*-indazole assumes a bidentate-chelated coordination mode (C,N); the two rings of the 2*H*-indaozle and phenyl moieties are coplanar. An in-depth investigation of the structural characteristics for all of the reported complexes (**4a−d** and **5a−d**) was carried out through computational methods using the B3LYP functional and DEF2-TZVPP basis set for ligands and atoms and SDD for Ir and Ru. The computed results were compared with the corresponding X-ray crystallographic data (Table S10).

The electronic properties of all of the complexes were studied in different solvents of varying polarity and protic

https://doi.org/10.1021/acs.inorgchem.1c02193
Inorg. Chem. 2021, 60, 17593−17607

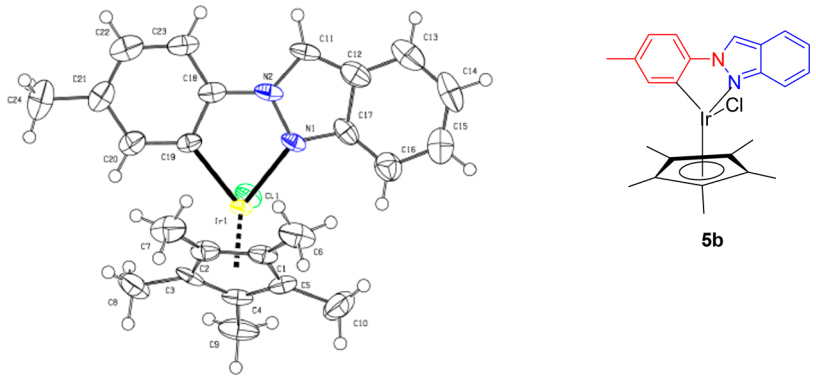

Figure 1. Single-crystal ORTEP diagram of compound **5b** (50% thermal ellipsoids). Selected bond lengths (angstroms) and angles (degrees) for **5b**: Ir−C19, 2.052(5); Ir−N1, 2.081(4); Ir−Cl, 2.408(11); Ir−Cp*(centroid), 1.81(2); C19−Ir−N1, 77.2(18); N1−Ir−Cl, 85.49(11); C19−Ir−Cl, 88.67(13); Cp*(centroid)−Ir−Cl, 92.6(13); Cp*(centroid)−Ir−N1, 143.6(19); Cp*(centroid)−Ir−C19, 139.1(2). CCDC number 2056445.

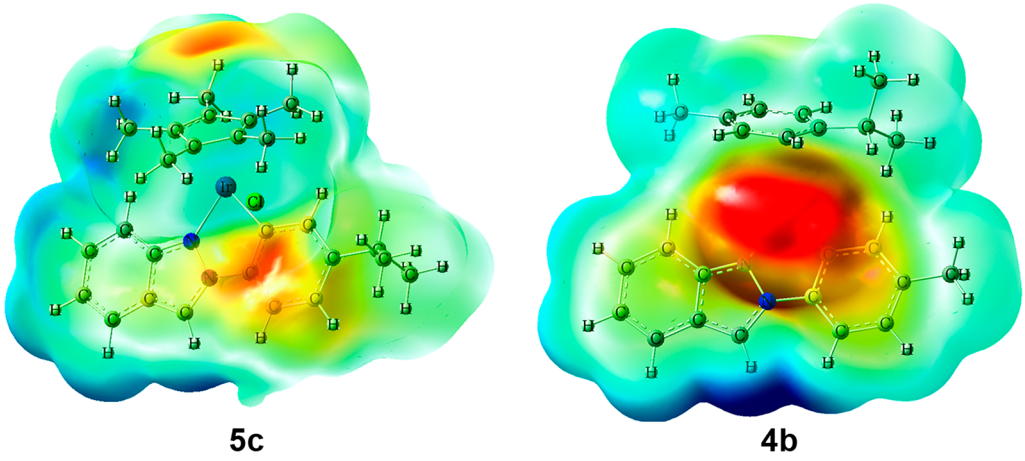

Figure 2. Computed (B3LYP/def2TZVPP) ESP surface maps drawn onto a total electron density surface (isovalue of 0.0004) and scaled between the electrostatic potential of $\pm 3.948 \times 10^{-2}$ au for iridium complexes (**5c**) and $\pm 4.118 \times 10^{-2}$ au for ruthenium complexes (**4b**). Red-colored surfaces are more positive electrostatic potential, and blue-colored surfaces more negative electrostatic potential.

nature to investigate their applications as potential optical probes, as well as in photodynamic therapy for cancer treatments. Stock solutions (5 mM) of **4a−d** and **5a−d** for the study were prepared in neat methanol, and further dilutions to achieve the working concentration of ∼5 μM in the respective solvent were carried out after evaporating the residual methanol. The electronic spectra of complexes **4a−d** and **5a−d** could not be recorded in water due to their poor solubility, and hence, the spectra had to be recorded in neat water with saturated aqueous solutions of the complexes. All other experiments in aqueous medium were performed in the presence of 5% DMSO to solubilize the complexes.

The ultraviolet−visible absorption spectra in various solvents like CH_2Cl_2 DMF, ethyl acetate, methanol, and water in the range of 220−450 nm were recorded to investigate their solvatochromic effect, and the results are depicted in Figure S2. The long wavelength absorption band of ruthenium complexes **4a−d** was centered at ∼280 and 330 nm, and that of iridium complexes **5a−d** at ∼280 nm. The spectra of ruthenium complexes were relatively more structured than those of iridium complexes, indicating the influence of solvents on perturbing various electronic levels to increase degeneracy. The short wavelength absorption band corresponds to the intraligand transitions, while the transitions that correspond to the long wavelength absorption band centered ∼330 nm are caused by the d−d transition, as evidenced by the low molar extinction coefficient values of ∼200 M^{-1} cm^{-1}. Moreover, the values of the molar extinction coefficient, as given in Table S1, indicate that the observed transitions are of a $\pi-\pi^*$ nature.

The fluorescence spectra of complexes **4a−d** and **5a−d** in different solvents as mentioned above were recorded in the range of 330−550 nm and at an excitation wavelength of 300 nm. Unlike the absorption spectra, a prominent shift was observed in the emission band maxima in different solvents with different polarities and protic natures (Figure S2). The results indicate the influence of dielectric parameters on stabilizing the various electronic levels of the complexes. An increase in the quantum yield was observed with an increase in the polarity of the solvents, and the values are listed in Table S1. The full width at half-maximum (fwhm) revealed that the observed band corresponds to a single species in the excited state in all of the solvents except for CH_2Cl_2. This could be due to the formation of additional species whose electronic transitions overlap with each other in the excited state. The same was also revealed from the excitation spectrum, where different band maxima were observed when spectra were recorded at different emission wavelengths (data not shown), indicating that the emission band in CH_2Cl_2 has two different originating species.

To investigate the stability of synthesized complexes **4a−d** and **5a−d** in aqueous medium, the absorption spectra were recorded in water with 5% DMSO at different time intervals (0

https://doi.org/10.1021/acs.inorgchem.1c02193
Inorg. Chem. 2021, 60, 17593−17607

Table 1. Cytotoxicities of Synthesized Compounds against Different Cell Lines [IC_{50} (micromolar)][a]

compound	MDA-MB-231 (SI)[b]	MDA-MB-468 (SI)[b]	HCT-116 (SI)[b]	HEK 293
1a	74.03 ± 2.78 (1.35)	65.43 ± 3.75 (1.52)	76.26 ± 1.20 (1.31)	>100
1b	29.23 ± 1.52 (3.42)	22 ± 1.46 (4.54)	63.08 ± 0.72 (1.58)	>100
1c	19.29 ± 0.41 (3.98)	18.94 ± 0.66 (4.03)	22.65 ± 0.84 (3.37)	76.49 ± 1.48
1d	>100 (~1)	71.1 ± 0.79 (1.34)	>100 (~1)	95.92 ± 2.52
4a	37.14 ± 1.95 (1.04)	22.96 ± 0.25 (1.68)	40.3 ± 1.19 (~1)	38.53 ± 1.04
4b	1.36 ± 0.74 (25.58)	1.69 ± 0.25 (20.57)	1.3 ± 0.003 (26.75)	34.78 ± 0.49
4c	4.97 ± 0.56 (6.65)	4.20 ± 0.07 (7.86)	6.03 ± 0.10 (5.48)	33.03 ± 1.02
4d	11.12 ± 0.20 (1.61)	5.15 ± 0.11 (3.47)	9.43 ± 0.19 (1.89)	17.85 ± 0.40
5a	3.33 ± 0.09 (7.19)	0.95 ± 0.03 (25.2)	3.47 ± 0.11 (6.90)	23.95 ± 0.28
5b	2.77 ± 0.06 (8.27)	0.75 ± 0.06 (30.56)	1.59 ± 0.04 (14.41)	22.92 ± 0.02
5c	1.19 ± 0.05 (15.6)	0.52 ± 0.02 (35.71)	1.36 ± 0.01 (13.65)	18.57 ± 0.05
5d	5.07 ± 0.11 (3.39)	4.13 ± 0.08 (4.17)	5.4 ± 0.09 (3.19)	17.23 ± 0.12
cisplatin	4.95 ± 0.05	2.27 ± 0.03	1.89 ± 0.06	9.89 ± 0.05

[a]Cells were incubated with the indicated compounds for 48 h. Data are presented as the means ± standard deviations, and cell viability was assessed after incubation for 48 h. [b]Selectivity Index.

and 24 h) in the presence and absence of 150 mM NaCl (Figure S3). We could see that the stabilities of iridium complexes (**5a−d**) were quite high under the conditions described above, while in the case of ruthenium complexes (**4a−d**), a hypochromic shift in the absorption band was observed, indicating their relatively poor stability in an aqueous environment. To ascertain these observations, the ^{1}H NMR spectrum of complex **5c** in a 10% DMSO/D_2O solvent mixture was recorded and no significant changes in the spectral pattern were observed even after 48 h, suggesting that the M−L bonds from the complexes are intact (Figure S5). The stability of all of the complexes was investigated in aqueous medium in the presence and absence of chloride ions. In addition, to further mimic the cellular and physiological conditions the stability was analyzed in the presence of 1 mM GSH and 150 mM NaCl. The relevant results are shown in Figure S4. It could be observed that the iridium complexes exhibited higher stability in the presence and absence of NaCl and GSH. It was also revealed that these complexes possess the ability to react with intracellular nucleophiles and are proposed as potential candidates for various therapeutic applications. Therefore, further investigations of anticancer potentials were limited to iridium complexes.

2.2. Electrostatic Potential Surface. To understand the influence of peripheral substitution at the C,N-cyclometalated ligand on the activity of complexes, quantum chemical calculations were performed on C−N cyclometalated ruthenium(II) (**4a−d**) and iridium(III) complexes (**5a−d**) featuring H, methyl, and isopropyl (electron-donating groups) and trifluoromethyl (electron-withdrawing group) groups at position 4 of the phenyl ring. Electrostatic potential (ESP) surfaces for all of the substitution patterns are shown in Figure S6.

The localized natural charge on the metal atom is higher for **5c** and **4b** (0.1716 and 0.3060, respectively) than for all of the reported complexes. Also, mapping of the ESP for complexes **5c** and **4b** as shown in Figure 2 displays lower electron density at the phenyl ring in comparison to that of the N-donor 2*H*-indazole ring system, which could be probably due to the peripheral substitution in the phenyl ring. In addition, the observed electron density on the indazole moiety is more prominent for the iridium complex than for the ruthenium complexes.

2.3. Cellular Kinetics and Uptake Characteristics. The synthesis and characterization of the cellular uptake properties of metal complexes were investigated in 2*H*-indazole iridium(III) (**5a−d**) complexes, and their potential was compared with that of their ruthenium(II) counterparts. Parameters like lipophilicity, nature of the substituent, and molecular size play crucial roles in determining the cellular uptake ability or the drug likelihood of synthesized complexes. To estimate the lipophilicity of the complexes, the conventional shake flask method was employed to follow their partition coefficients in *n*-octanol/water ($P_{o/w}$).[29] It was also revealed in the stability studies described above that iridium complexes are not hydrolyzed under aqueous and physiological conditions. In addition, the cellular uptake efficacies of **4b** and **5c** were determined in MDA-MB-468 cell lines using inductively coupled plasma mass spectrometry (ICP-MS) as shown in Figure S7. The result has revealed a disproportionate concentration dependence in cellular accumulation. In the case of iridium(III) complexes, the uptake potentials of **5c** per 10^6 cells were observed to be 0.186 μg at 3 μM and 0.274 μg at 10 μM, while in the case of ruthenium(II) complexes, **4b** revealed potentials of 0.061 μg at 5 μM and 0.0791 μg at 10 μM. Moreover, the uptake kinetics was also assessed by the observed time-dependent increase in cytotoxicity by following the MTT proliferation studies.

2.4. *In Vitro* Cytotoxicity. Generally, low cytotoxicity toward noncancerous cells and specific killing of malignant cells are prerequisites for an ideal antineoplastic drug. Assessing quantitatively the mitochondrial integrity through a 3-(4,5-dimethylthiazol-2-yl)-2,5-diphenyltetrazolium bromide (MTT) assay serves as the effective strategy while screening for the cellular proliferative index in a multitude of cytotoxic ligands. With the multiwall format and with a change in the treatment intervals, the variation in cancer cell proliferation can be efficiently quantified using the MTT assay. In this study, the *in vitro* cytotoxicity of ruthenium(II) (**4a−d**) and iridium(III) (**5a−d**) was evaluated by the MTT assay along with cisplatin as a positive metallo-drug against MDA-MB-231, MDA-MB-468 (TNBC cells), and HCT-116 (human colon cancer cell) cells and compared with the cytotoxicity against noncancerous HEK 293 (human embryonic kidney) cells. After treatment for 48 h, all of the complexes exhibit high cytotoxicity with favorable IC_{50} values, which is even better than those of cisplatin against all human cancer cell lines tested (Table 1). It

https://doi.org/10.1021/acs.inorgchem.1c02193
Inorg. Chem. 2021, 60, 17593−17607

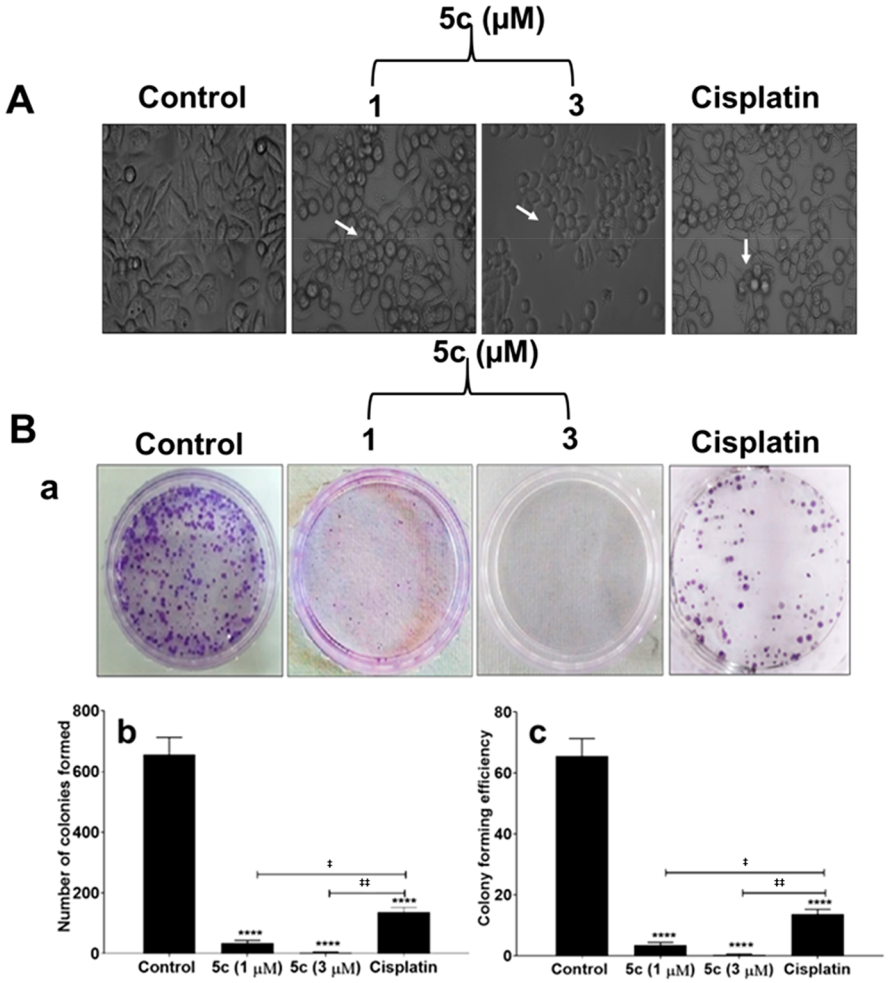

Figure 3. Complex **5c** induced morphological changes and inhibited colony formation ability in TNBC cells. (A) Images representing morphological changes induced by complex **5c** at the indicated concentrations after treatment for 24 h. (B) (a) Representative images of a clonogenic survival assay of MDA-MB-468 cells and (b and c) histograms representing the colony number and colony forming efficiency, respectively, of MDA-MB-468 cells. The figures depicted are representative of three independent experiments. Results are represented as means ± standard deviations (SD), and asterisks and double daggers denote values significantly different from those of the control and cisplatin respectively, $*/^{\ddagger}p < 0.05$. $**/^{\ddagger\ddagger}p < 0.01$. $****/^{\ddagger\ddagger\ddagger\ddagger}p < 0.0001$.

was revealed that the cytotoxic activities of iridium(III) (**5a–d**) complexes were higher than those of ruthenium(II) (**4a–d**) complexes. In particular, complex **5c** exhibited significantly lower IC_{50} values against MDA-MB-231 (1.19 ± 0.05 μM), MDA-MB-468 (0.52 ± 0.026 μM), and HCT-116 (1.36 ± 0.01 μM) cells. Also, the cytotoxocity results clearly revealed the specificity of **5c** for cancer cells over noncancerous cells. This highlights the specificity of these metal drug complexes toward fast-growing cancer cell lines rather than the normal noncancerous cells. The iridium(III) (**5a–d**) complexes showed good cytotoxicity against cancer cells compared to that of cisplatin.

Among the synthesized complexes, iridium(III) (**5a–d**) complexes exhibited prominent antitumor activity. The data in Table 1 revealed **5c** to be the most effective with consistent cytotoxicity against the MDA-MB-468 cell line.

To further confirm the cytotoxicity of Ir(III) complexes (**5a–d**) and Ru(II) complex **4b** against MDA-MB-468 cells, we have investigated the drug-induced morphological changes under a phase-contrast microscope. As shown in Figure 3A, in comparison with cisplatin, the cells treated with **5c** (1 and 3 μM) exhibited significant alterations in their morphology. The treated cells appeared to be round with subsequent detachment and cell death. The same was observed in cells treated with **5a** (2.3 μM), **5b** (3.5 μM), and **5d** (8.2 μM) for 24 h, as shown in Figure S8A. Similar morphological changes were also observed in the case of **4b**, and the same is depicted in Figure S9. The observations were more pronounced with increasing concentrations of **5c**. The results were compared with those of vehicle control-treated cells that stayed healthy and did not exhibit cell death. Aggressive TNBC cells undergo uncontrolled cell division and thus have the ability to produce colonies even when plated at a lower cell density. Usually, this colony forming ability could be related to their proliferative index and is monitored to check the mitotic ability of cancer cells after treatment with test compounds or ionizing radiation.[30] MDA-MB-468 cells treated with **5c** (1 and 3 μM) for 24 h showed a significant reduction in colony number and in the size of the colonies in a concentration-dependent manner compared to the values of the control and cisplatin-treated cells as shown in Figure 3B.

The highest concentration (3 μM) almost abolished the ability of TNBC cells to form colonies. Thus, it can be inferred that Ir(III) complex **5c** exerted both cytotoxic and cytostatic

https://doi.org/10.1021/acs.inorgchem.1c02193
Inorg. Chem. 2021, 60, 17593–17607

activities. While the improved efficacy of platinum drugs was explored,[31] an attempt to use novel C−N cyclometalated 2*H*-indazole iridium(III) complexes could enhance the availability of ligand-conjugated metallo-drug options for the treatment of TNBC cells.

2.4.1. Determination of Intracellular Reactive Oxygen Species (ROS). With respect to metal drugs, the generation and upregulation of intracellular ROS play an important role while initiating apoptosis through both intrinsic and extrinsic apoptotic pathways.[32,33] An increased level of mitochondrial ROS can damage mtDNA and thereby induce the mitochondrion-mediated intrinsic apoptotic pathway in cancer cells.[34] ROS-based therapeutics are well recognized both in classical chemotherapy and with the recent targeted approaches.[35]

To investigate the possibility of ROS generation upon treatment of MDA-MB-468 cells with iridium(III) complex **5c**, we used the cell-permeable, ROS specific dye DCFDA (2′,7′-dichlorofluorescein diacetate). The DCFDA dye will be converted to nonfluorescent DCFH by cellular esterases, which is then subsequently oxidized to highly fluorescent DCF in the presence of ROS. As shown in Figure 4, only the

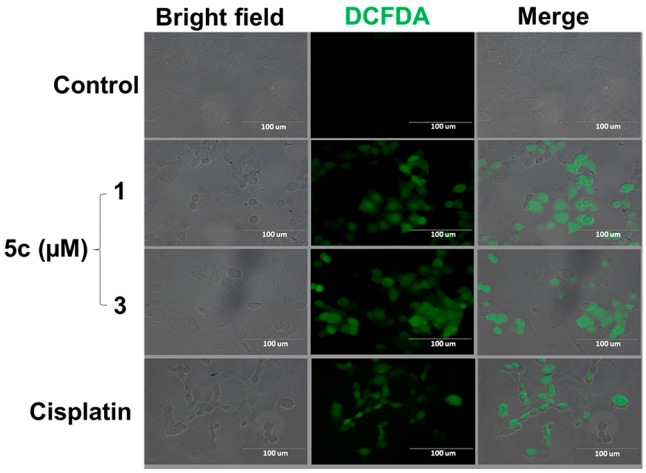

Figure 4. Complex **5c** induced generation of ROS in TNBC cells. The generation of subcellular ROS was analyzed by fluorescence microscopy with DCFDA staining. The generated ROS levels were higher in the complex **5c** (1 and 3 μM) and cisplatin (5 μM) treatment groups than in the untreated control. This figure is representative of three independent experiments (scale bar, 100 μm).

background fluorescence was observed in control untreated cells while in cells treated with **5c** (1 and 3 μM), the fluorescence was visibly enhanced, indicating the increase in the level of ROS induced by **5c** in MDA-MB-468 cells.

Similar results were seen for cells treated with cisplatin (5 μM). Effectively, the treatment with **5c** substantially induced generation of ROS, which lead to oxidative stress and eventually the death of MDA-MB-468 cells. We have also analyzed other iridium(III) complexes such as **5a** (2.3 μM), **5b** (3.5 μM), and **5d** (8.2 μM) for their ability to increase the level of ROS as depicted in Figure S8B in the TNBC cell line and found that all of the iridium(III) complexes are capable of increasing the level of ROS when used at their IC_{50} concentrations.

2.4.2. Apoptotic Study. Escaping apoptosis is one of the important properties of cancer cells, which leads to uncontrolled cell proliferation and the development of resistance to various therapies. TNBC cells frequently develop resistance to chemotherapeutic agents by overriding apoptosis and become unresponsive to treatment modalities.[36,37] Compared to cisplatin, in MTT and other assays, iridium complexes were highly effective in inducing cell death. Thus, it is possible that iridium(III) complex **5c** might effectively induce apoptosis in the tumor cell, which could be an effective strategy for targeting TNBC. The flipped exposure of phosphatidylserine (PS) to the outer side of the cell membrane is a general marker for apoptosis. To determine whether cell death induced by **5c** on MDA-MB-468 cell lines occurs via apoptosis or necrosis, we carried out quantitative analysis of phosphatidylserine externalization by flow cytometry using Annexin V as an apoptosis marker. The different cell populations gated and tracked by this method were Q1-LL Live [Annexin V^-/PI^-), Q1-LR Early apoptosis (Annexin V^+/PI^-), Q1-UR Late apoptosis (Annexin V^+/PI^+), and Q1-UL Necrotic (Annexin V^-/PI^+). Compared to the control and cisplatin (5 μM) treatment groups, there is a striking increase in the percentage of early and late apoptotic cell populations in **5c**-treated groups (Figure 5A). Also there is a significant concentration-dependent increase in positive apoptotic populations with **5c**-treated cells (Figure 5B). At the lower concentration of **5c** of 1 μM, ∼18.75% and ∼16.20% of the cells were found to be in early and late apoptotic stages, respectively. Significantly, on the contrary, treatment with 3 μM complex **5c** shows 7.49% and 76.03% of the cells were found to be in early and late apoptotic stages, respectively.

A small fraction of the population (4.30% and 2.54%) was found to be of necrotic cells in the two concentrations of Ir conjugates applied. In comparison, cells treated with 5 μM cisplatin showed 10.77% early apoptotic cells, 13.15% late apoptotic cells, and 3.98% necrotic cells. Thus, the cytotoxic effects seen with Ir-complexed 2*H*-indazoles were very similar to or in some cases more efficient than those of the platinum drugs. A small proportion of necrotic cells (4.30% and 2.54% at 1 and 5 μM, respectively) were seen in cells treated with **5c**. In comparison, cisplatin-treated cells showed 10.77%, 13.5%, and 3.98% early apoptotic, late apoptotic, and necrotic cells, respectively.

Mitochondria are said to be the energy reservoir of the cells and the site of ATP synthesis. Cancer cells have the ability to beneficially alter cellular energetics by altering mitochondrial metabolism. This aberrant energetic process influences the growth, division, tumor progression, and even drug response and thus makes mitochondria potential targets for anticancer drug discovery.[34,38,39] It has been reported that metal-based anticancer drug cisplatin exerts its effects by targeting nuclear DNA and can provoke drug resistance by interfering with DNA repair mechanisms.[34] However, other metal complexes, with distinct modes of action compared to that of cisplatin, could overcome this possibly by targeting other molecules.[40] Interestingly, mitochondrial DNA (mtDNA) is highly vulnerable when treated with transition metals and could become an effective target due to the lack of a repair mechanism and histone protection.[19,34] It is well-known that the mitochondrial damage and loss of the mitochondrial membrane potential ($\Delta\Psi_m$) are said to be early events in the mitochondrion-mediated apoptosis pathway and considered to be a hallmark for apoptosis. The cells with a decreased $\Delta\Psi_m$ can irreversibly enter apoptosis by causing the release of cytochrome *c* and activating caspases.[38] Previous reports suggested that Ir(III) complexes can evoke ROS generation and also reduce the $\Delta\Psi_m$ to exert pro-apoptotic properties

https://doi.org/10.1021/acs.inorgchem.1c02193
Inorg. Chem. 2021, 60, 17593−17607

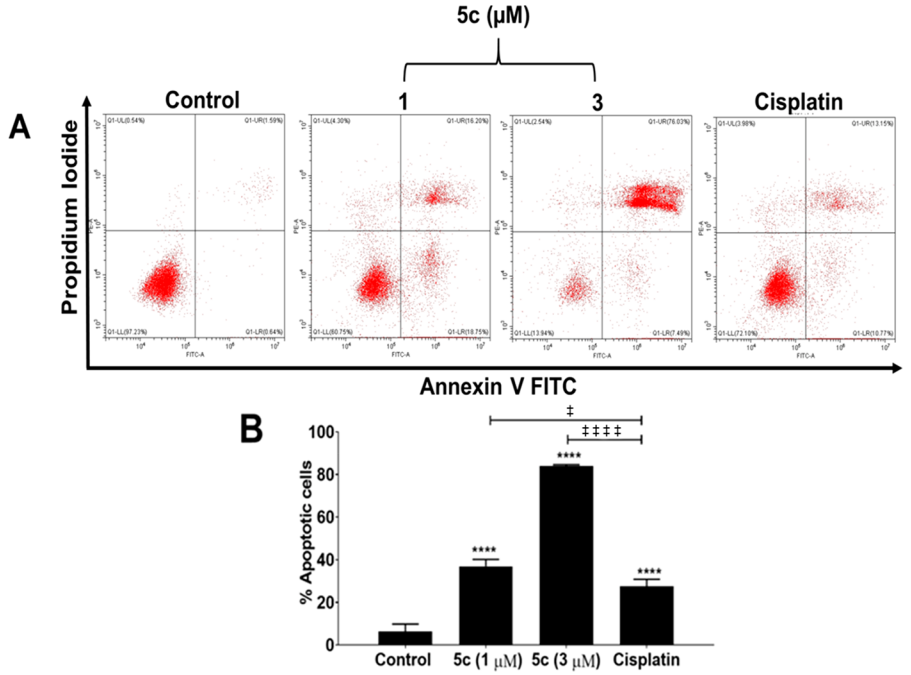

Figure 5. Complex **5c** induced apoptosis in triple negative breast cancer (TNBC) cells. (A) Flow cytometry analysis of apoptosis by Annexin V FITC and PI. MDA-MB-468 cells treated with control, **5c** (1 and 3 μM), and cisplatin (5 μM) for 24 h. The histograms represent the distribution of cells in live, early apoptosis, late apoptosis, and necrotic phases. (B) Bar diagram representing the percentage of apoptotic cells. Results are represented as mean ± SD, and asterisks and double daggers denote values significantly different from those of the control and cisplatin, respectively. */$^{\ddagger}p < 0.05$. ****/$^{\ddagger\ddagger\ddagger\ddagger}p < 0.0001$.

simultaneously.[22,34,41−44] Thus, to reveal the involvement of the mitochondrial apoptotic pathway exerted by **5c** and the associated change in $\Delta\Psi_m$, TNBC cells were subjected to JC-1 staining-based characterization. This cationic dye selectively accumulates as J-aggregates that emit red fluorescence in healthy cells and remain in the monomeric form, which emits green fluorescence, in apoptotic cells due to the decreased membrane potential.[45] From Figure 6A, it is clear that cells treated with **5c** showed concentration-dependent changes in $\Delta\Psi_m$, and these changes are more prominent than those of cisplatin-treated cells. On the contrary, untreated cells emitted red fluorescence indicative of healthy mitochondria, thereby revealing the prominent role played by the mitochondrial apoptosis during iridium(III)-conjugated 2*H*-indazole toxicity.

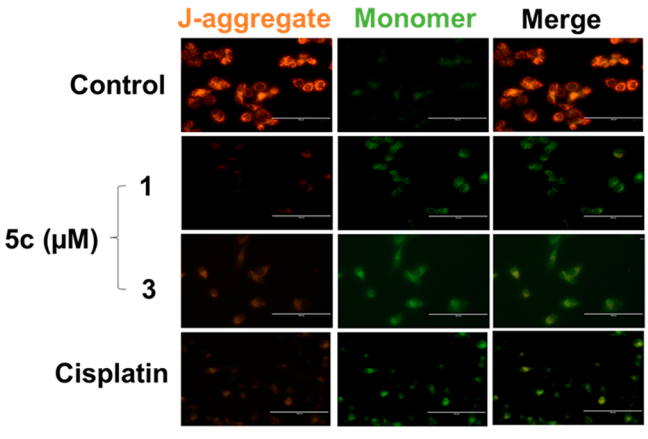

Figure 6. Complex **5c** induced mitochondrion-mediated apoptosis in triple negative breast cancer (TNBC) cells. Fluorescence microscopy images of mitochondrial membrane potential changes analyzed by JC-1 staining. MDA-MB-468 cells showed a decreased $\Delta\Psi_m$ after being treated with complex **5c** (1 and 3 μM) compared with those of untreated cells (Control) and cells treated with cisplatin (5 μM) for 24 h. The figures are representative of three independent experiments (scale bar, 100 μm).

2.4.3. Enhanced Activation of Caspase 3 by Ir(III) Complex ***5c****.* When the mitochondrial $\Delta\Psi_m$ is disrupted, the release of cytochrome *c* triggers a cascade of events that eventually activates caspases and leads to apoptotic cell death. During apoptosis, cells undergo distinct morphological changes like cell shrinkage, chromatin condensation, nuclear fragmentation, outer membrane blebbing, and changes in the cytoskeletal dynamics that are mediated by active execution caspases. The activation of caspase 3 represents an early event of apoptosis, which plays an important role in the subsequent execution of apoptosis by cleaving key structural proteins associated with nuclear, mitochondrial, and cytoskeletal integrity, thus leading to apoptotic cell death.[46,47] To confirm the involvement of caspase activation, and thereby the mitochondrial route of intrinsic apoptosis in complex **5c**-induced cell death, we next examined the activation of caspase 3/7 by using CellEvent Caspase-3/7 Green ReadyProbes. This probe has the inhibitory DEVD peptide bound to the fluorochrome, thus preventing it from binding to DNA in the healthy cells. However, upon activation of caspase 3/7 in apoptotic cells, activation-linked cleavage of the DEVD peptide in turn releases the fluorochrome, which readily enters the nucleus and emits green fluorescence. In this study, the MDA-MB-468 cells treated with complex **5c** (1 and 3 μM) and cisplatin (5 μM) for 24 h showed bright green fluorescence, which indicates the activation status of caspase 3/7 as in Figure 7. The absence of any fluorescence in the untreated cells confirms the complex **5c** specific, caspase-mediated cellular apoptosis in TNBC cells. Caspase 3/7 activation was also

https://doi.org/10.1021/acs.inorgchem.1c02193
Inorg. Chem. 2021, 60, 17593−17607

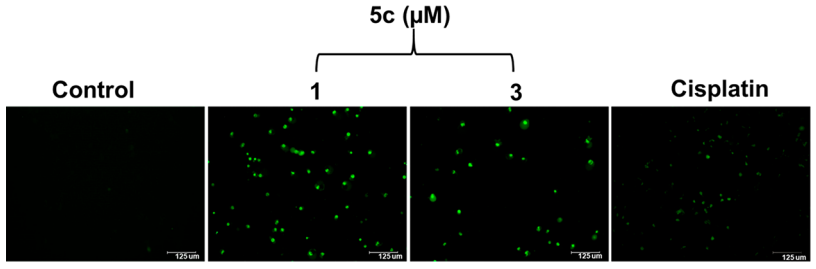

Figure 7. Complex **5c** induced caspase 3/7 activation in triple negative breast cancer (TNBC) cells. Fluorescence microscopy images of caspase 3/7 activation in MDA-MB-468 cells treated with complex **5c** for 24 h. The cells treated with complex **5c** (1 and 3 μM) and cisplatin (5 μM) showed bright green fluorescence, which indicates the binding of free nucleic acid dye to the DNA upon clevage of inhibitory DEVD peptide by activated effector caspases 3/7. Where as in untreated (Control) cells there was no fluorescence was observed. The figures are representative of three independent experiments (scale bar, 125 μm).

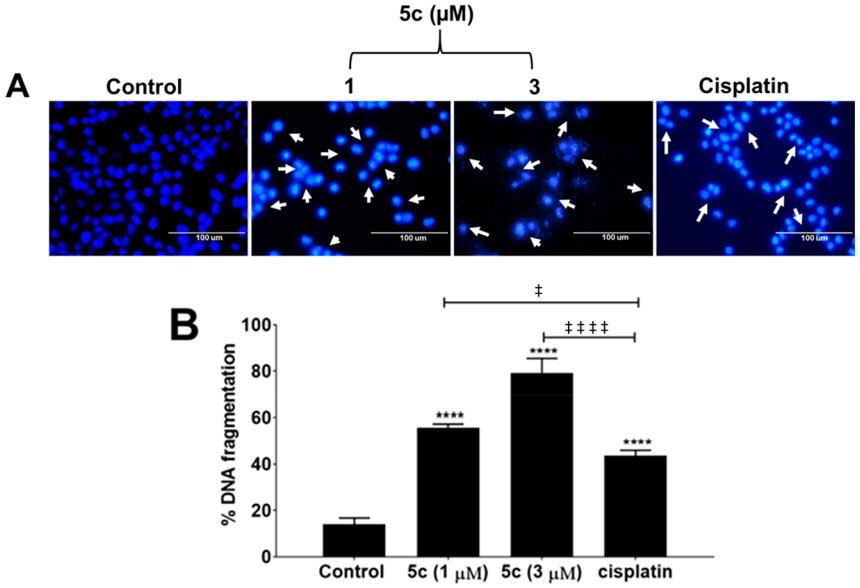

Figure 8. Complex **5c** induced nuclear fragmentation in triple negative breast cancer cells. (A) Representative images of DAPI staining of cells treated with complex **5c** (1 and 3 μM) and cisplatin (5 μM) that showed an altered nuclear morphology and nuclear fragmentation indicated with white arrows compared to control cells. Representative images shown from three or more independent experiments. (B) Bar diagram representing the quantification of DNA fragmentation by the diphenylamine (DPA) method. Results are represented as means ± SD. Asterisks and double daggers denote values significantly different from those of the control and cisplatin, respectively. */$^{‡}p$ < 0.05. ****/$^{‡‡‡‡}p$ < 0.0001 (scale bar, 100 μm).

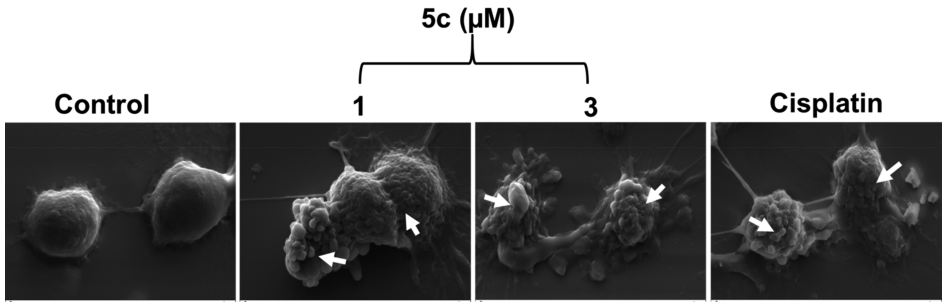

Figure 9. Complex **5c** induced cell membrane blebbing in triple negative breast cancer cells. Scanning electron microscopy images of the formation of membrane blebs in MDA-MB-468 cells treated with complex **5c** for 24 h. Control cells show a smooth cell surface, whereas the cells treated with complex **5c** (1 and 3 μM) and cisplatin (5 μM) show an altered morphology with the formation of cell membrane blebs. White arrows indicate cellular blebbing. Representative images shown from three independent experiments (magnification, 15.00K×).

observed in the cells treated with iridium(III) complexes **5a** (2.3 μM), **5b** (3.5 μM), and **5d** (8.2 μM) at their respective IC_{50} concentrations for 24 h as shown in Figure S8C, which indicated the apoptotic induction ability of the iridium(III) complexes in TNBC cells.

To further verify and visually confirm the complex **5c**-induced apoptotic cell death, w also studied the effect of complex **5c** on the nuclear morphology of MDA-MB-468 cells using DAPI staining (Figure 8A). The cells incubated with complex **5c** (1 and 3 μM) for 24 h showed changes in nuclear

https://doi.org/10.1021/acs.inorgchem.1c02193
Inorg. Chem. 2021, 60, 17593−17607

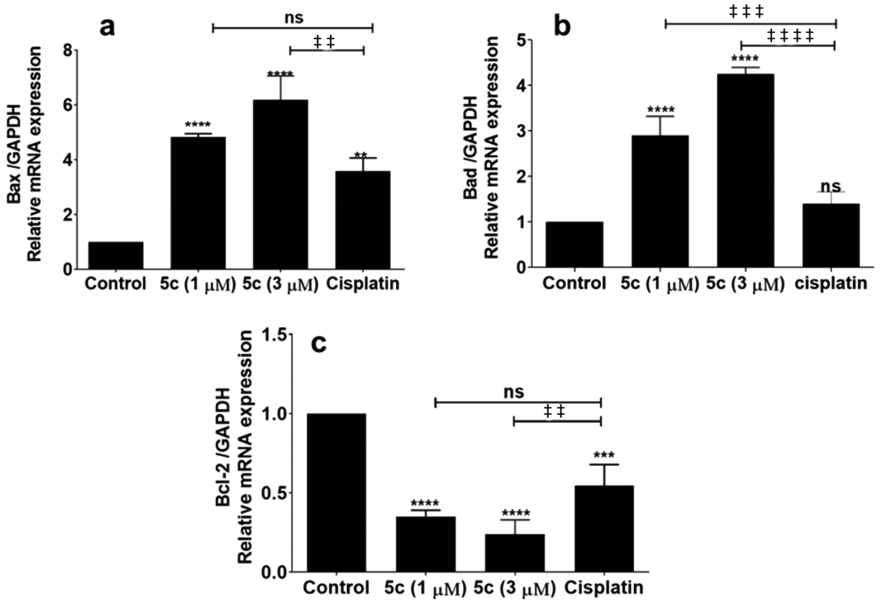

Figure 10. Complex **5c** induced changes in the expression levels of pro- and antiapoptotic proteins. Real time PCR analysis of (a) Bax, (b) Bad, and (c) Bcl-2 mRNA expression in MDA-MB-468 cells treated with complex **5c** (1 and 3 μM) and cisplatin (5 μM) for 24 h and the control. The mRNA levels are normalized to internal control GAPDH and displayed as the fold change. The results are expressed as means ± SD. Asterisks and double daggers denote values significantly different from those of the control and cisplatin, respectively. **/$^{‡‡}p$ < 0.01. ***/$^{‡‡‡}p$ < 0.001. ****/$^{‡‡‡‡}p$ < 0.0001. ns indicates nonsignificant data.

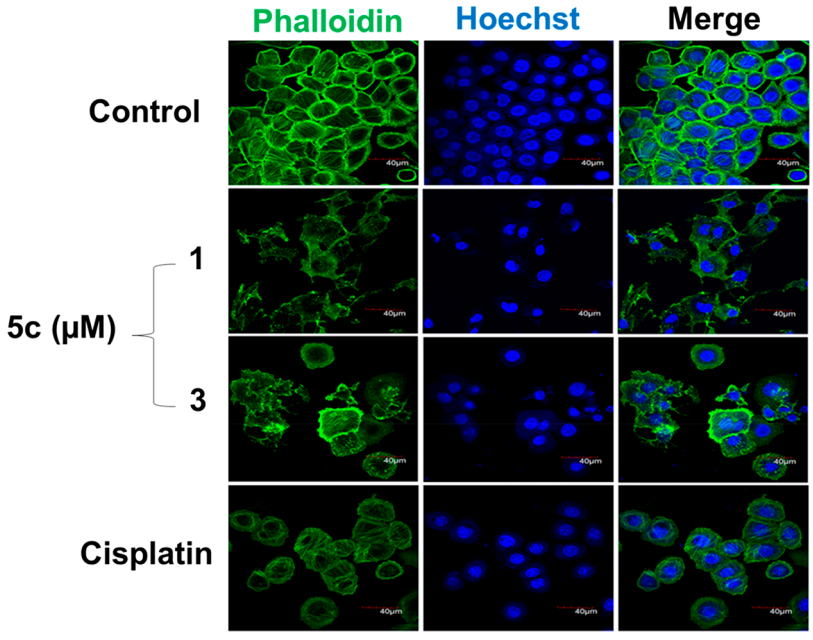

Figure 11. Complex **5c** induced changes in the actin cytoskeleton structure in TNBC cells. Confocal microscopy images of phalloidin staining show changes in the actin cytoskeleton in MDA-MB-468 cells treated with complex **5c** (1 and 3 μM) and cisplatin (5 μM) for 24 h and control cells. Complex **5c** induced F-actin remodeling and morphological changes in MDA-MB-468 cells. Representative images shown from three or more independent experiments (scale bar, 40 μm).

morphology, typically with more condensed and fragmented nuclei compared with cells treated with cisplatin (5 μM). However, the untreated control cells possessed healthy nuclear staining. A similar nuclear morphology and similar condensation were also observed in the cells treated with iridium(III) complexes **5a** (2.3 μM), **5b** (3.5 μM), and **5d** (8.2 μM) at their respective IC_{50} concentrations for 24 h as shown in Figure S8D. The apoptotic effect of complex **5c** on MDA-MB-468 cell lines was also quantitatively confirmed using the diphenylamine (DPA) method (Figure 8B). The results indicate that the percentage of fragmented DNA significantly increases in a concentration-dependent manner in cells treated with complex **5c** (1 and 3 μM) compared to those of the control and cells treated with cisplatin (5 μM). This indicates that the extent of apoptosis induced by Ir(III) complex **5c** is high compared to that of the standard anticancer drug cisplatin.

https://doi.org/10.1021/acs.inorgchem.1c02193
Inorg. Chem. 2021, 60, 17593−17607

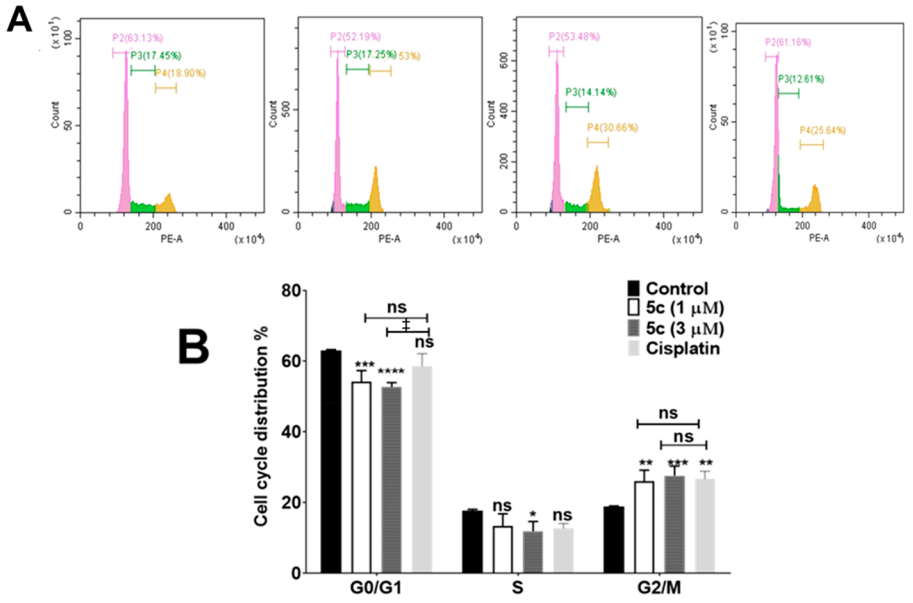

Figure 12. Complex **5c** induced G2/M phase cell cycle arrest in TMBC cells. (A) Representative results of cell cycle analysis from a flow cytometer assay in MDA-MB-468 cells treated with complex **5c** (1 and 3 μM) and cisplatin (5 μM) for 24 h and the control. (B) Bar diagram representing the G0/G1, S, and G2/M phase proportions of MDA-MB-468 cells. Data shown are representative of three independent experiments. Results are represented as means ± SD. Asterisks and double daggers denote values significantly different from those of the control and cisplatin, respectively. */$^{‡}p$ < 0.05. **/$^{‡‡}p$ < 0.01. ***/$^{‡‡‡}p$ < 0.001. ****/$^{‡‡‡‡}p$ < 0.0001. ns indicates nonsignificant data.

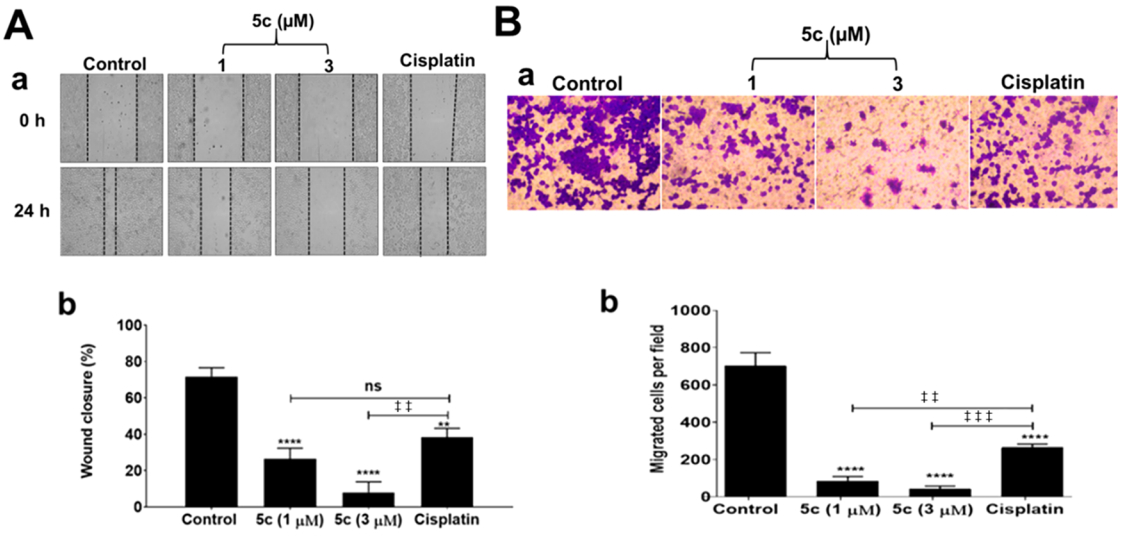

Figure 13. Complex **5c** attenuated the cellular migration ability of triple negative breast cancer cells. MDA-MB-468 cells were treated with different concentrations of complex **5c**, and cell migration was examined by a wound healing assay and a transwell migration assay. (A) (a) Representative microscopic images of wound healing in which the dotted lines represent the borders of the wound. (b) Bar diagram representing wound closure percentages. The open wound area was measured by ImageJ software, and the percentage of wound closure was calculated and is represented in bar diagrams. (B) (a) Representative images of a transwell migration assay. (b) Bar diagrams representing the number of migrating cells per field. Representative images are shown from three or more independent experiments. Results are represented as means ± SD. Asterisks and double daggers denote values significantly different from those of the control and cisplatin, respectively. **/$^{‡‡}p$ < 0.01. ***/$^{‡‡‡}p$ < 0.001. ****/$^{‡‡‡‡}p$ < 0.0001. ns indicates nonsignificant data.

Cell membrane blebbing is one of the hallmarks of apoptosis. To visualize cell membrane blebbing induced by complex **5c** in MDA-MB-468 cells, we next performed scanning electron microscopy. From Figure 9, it is evident that the cells treated with different concentrations of complex **5c** have undergone changes in the cell surface characterized by the formation of unique apoptotic membrane blebs. In contrast, the control cells appeared to be normal without the membrane blebs. Cell membrane blebs were also seen in cisplatin-treated cells. This result again visually indicates that complex **5c** is capable of causing apoptotic cell death in TNBC cells. The cell membrane blebs were also observed in the cells treated with iridium(III) complexes **5a** (2.3 μM), **5b** (3.5 μM), and **5d** (8.2 μM) at their respective IC_{50} concentrations for 24 h as shown in Figure S8E.

The induction of apoptosis by Ir(III) complex **5c** is evident from the increased mRNA levels of pro-apoptotic genes *Bax* and *Bad* and the reduced level of expression of antiapoptotic

https://doi.org/10.1021/acs.inorgchem.1c02193
Inorg. Chem. 2021, 60, 17593−17607

gene *Bcl-2* mRNA. From these results, it is evident that Ir(III) complex **5c** primarily induced mitochondrion-mediated apoptosis in MDA-MB-468 cells as shown in Figure 10.

2.5. Changes in Cytoskeletal Dynamics and Consequences. The changes in the cytoskeletal network in MDA-MB-468 cells treated with Ir(III) complex **5c** were observed by staining with F-actin using Alexa Fluoro 488 Phalloidin. The incubation of MDA-MB-468 cells with 1 and 3 μM complex **5c** strongly modified the structure of the actin cytoskeleton when compared to that seen in control and cisplatin-treated cells. These results suggest the cytoskeletal changes from collapsed actin networks are associated typically with apoptosis and are triggered by complex **5c** as shown in Figure 11.

2.5.1. Cell Cycle Arrest. Application of chemotherapeutic drugs usually arrests the cell cycle process and mediates cancer cell death due to insufficient DNA repair. To investigate whether Ir(III) complex **5c** modulates any cell cycle phase of MDA-MB-468 cells, we tracked cell cycle phases P2 (G0/G1 phase), P3 (S-phase), and P4 (G2/M phase) in the treated population by flow cytometry after propidium iodide (PI) staining (Figure 12). The results indicate that the cells treated with different concentrations of complex **5c** (1 and 3 μM) and cisplatin (5 μM) showed increased proportions of cells in G2/M phases when compared to control cells. In the control group, the proportions of cells present in each phase are 63.13%, 17.45%, and 18.90% in phases P2−P4, respectively. In the case of cells treated with complex **5c**, at 1 μM 52.19%, 17.25%, and 27.53% were in phases P2−P4, respectively, while at 3 μM 53.48%, 14.14%, and 30.66% were in phases P2−P4, respectively. This shows the significant concentration-dependent increase in arrested cells in the G2/M phase of the cell cycle upon treatment with complex **5c**. Cells treated with 5 μM cisplatin showed 61.16%, 12.61%, and 25.64% in phases P2−P4, respectively. This indicated that complex **5c** induced G2/M phase cell cycle arrest in MDA-MB-468 cells in a manner similar to that of cisplatin. Modulation of cell cycle arrest at the G2/M phase through enhancing the arrest or abrogating the arrest has been used to improve the cytotoxicity of therapeutic agents.[48] Interestingly, the enhanced G2/M arrest by 2*H*-indazole-ligated iridium(III) in MDA-MB-468 cells supports the view of G2/M arrest followed with the enhanced cytotoxicity by 2*H*-indazole conjugates.

2.5.2. Cell Migration. The process of metastasis involves spreading of the cancer cells from the primary tumor site to secondary sites, which is effected through cellular migration and invasion within circulatory systems and in the tissue matrix. We investigated the effect of Ir(III) complex **5c** on the cell migratory ability of MDA-MB-468 cells *in vitro* by performing a wound healing migration assay and a transwell migration assay. As shown in Figure 13A, complex **5c** inhibited the migratory potential of MDA-MB-468 cells, which is evident from the concentration-dependent decreased rate of wound closure compared to that of the control cells. Also, inhibition of wound closure is comparatively effective compared to than the positive control cisplatin treatment.

The transwell migration assay in Figure 13B suggests that the number of migrated cells was significantly decreased in cells treated with complex **5c** compared to that of the untreated control and that of the cisplatin treatment group. This indicates that complex **5c** is capable of inhibiting cellular migration of TNBC cells *in vitro*, and thus, it can alter the metastatic potential of this aggressive breast cancer cell type.

3. CONCLUSIONS

We have developed a successful divergent synthesis of novel C,N-cyclometalated 2*H*-indazole ruthenium(II) and iridium(III) complexes of the types $[(\eta^6\text{-}p\text{-cymene})RuCl(\text{-}N,C\text{-}2H\text{-indazole})]$ and $[(\eta^5\text{-}C_5Me_5)IrCl(\text{-}N,C\text{-}2H\text{-indazole})]$ with various substituents (H, Me, isopropyl, and CF_3) in the R_4 position of the phenyl ring of the 2*H*-indazole ligand of ruthenium (**4a−d**) and iridium complexes (**5a−d**). The structures of all complexes were unequivocally confirmed by ^{1}H NMR, ^{13}C NMR, HRMS, and elemental analyses. In addition, complex **5b** was confirmed by single-crystal X-ray diffraction analysis. The cytotoxic activity of the new ruthenium(II) and iridium(III) complexes has been evaluated in human cancer cell lines such as TNBC cell lines MDA-MB-231 and MDA-MB-468 and on colon cancer cell line HCT-116. Almost all new complexes have shown appreciable activity, comparable to or significantly better than that of cisplatin in TNBC cell lines. Increased potency was observed in Ir(III) complex **5c** when the R_4 substituent of the phenyl ring of the 2*H*-indazole ligand is an isopropyl group as compared to the parent compounds in all cell lines. Moreover, Ir(III) complex **5c** induced mitochondrial damage by generating large amounts of ROS, which triggered mitochondrion-mediated apoptosis in TNBC cell line MDA-MB-468. Moreover, complex **5c** also induced G2/M phase cell cycle arrest and inhibited cellular migration of TNBC cells. As reported recently for planar ligand-derived cyclometalated Ir(III) complexes by Cao et al.,[34] with our finding involving significant induction of ROS and mitochondrial disruption, it is possible that in addition to chromosomal DNA, targets like mtDNA damage might also play a key role in C,N-cyclometalated 2*H*-indazole Ir(III) complex-mediated toxicity. The Ir(III) complex reported herein could effectively target TNBC cells with high specificity. In general, this work provides strong evidence that Ir(III) complex **5c** could be further studied to explore the fullest anticancer potential as such or with few modifications. Also, it could be utilized as a potential mitochondrial targeting anticancer agent.

4. EXPERIMENTAL SECTION

4.1. Chemistry. *4.1.1. General Methods.* Unless otherwise indicated, all common reagents and solvents were used as obtained from commercial suppliers without further purification. ^{1}H NMR (400 MHz) and ^{13}C NMR (100 MHz) spectra were recorded on a Bruker DRX400 spectrometer. Chemical shifts are reported in parts per million relative to the internal solvent peak. Coupling constants, *J*, are given in hertz. Multiplicities of peaks are given as d (doublet), m (multiplet), s (singlet), and t (triplet). Mass spectra were recorded on a PerkinElmer Calrus 600 GC-MS spectrometer. Elemental analyses were carried out using a PerkinElmer 2400 Series II instrument. High-resolution mass spectra (HRMS) were recorded in ESI mode using a Thermo Exactive LC-MS mass spectrometer. Ultraviolet−visible spectroscopy was carried out on a UV-2550 instrument (Shimadzu Corp., Kyoto, Japan). Solvents were dried by the usual methods. $[(\eta^6\text{-}p\text{-Cymene})RuCl_2]_2$ and $[(\eta^5\text{-}C_5Me_5)IrCl_2]_2$ were obtained from Sigma-Aldrich (Bangalore, India). The syntheses of metal complexes **4a−d** and **5a−d** were carried out using the method reported in the literature with a slight modification.[28]

*4.1.2. General Procedure for the Synthesis of Substituted 2H-Indazole Ru(II) Complexes **4a−d**.* In a round-bottom flask equipped with a magnetic bar under a nitrogen atmosphere, 2-phenyl-2*H*-indazole (1 mmol) **1a** was dissolved in a freshly distilled dichloromethane solution (5 mL). Sodium acetate (1.2 mmol) was added to the flask at room temperature while its contents were being constantly stirred followed by the addition of $[(\eta^6\text{-}p\text{-cymene})RuCl_2]_2$ (0.5

https://doi.org/10.1021/acs.inorgchem.1c02193
Inorg. Chem. 2021, 60, 17593−17607

mmol) **2**. The reaction mixture was stirred at room temperature for 20 h, and the progress of the reaction was monitored by TLC. After the complex had formed, diethyl ether (10 mL) was added to the mixture. The reaction mixture was stirred for 10 min to precipitate the product. The crystalline product was filtered through a fritted funnel and dried well. Yellow-colored ruthenium complex **4a** was obtained in good yield (72%): R_f = 0.25 (40% EtOAc/*n*-hexane); ^{1}H NMR (400 MHz, $CDCl_3$) δ 8.43 (s, 1H), 8.23 (d, J = 7.2 Hz, 1H), 7.98 (d, J = 8.8 Hz, 1H), 7.66 (d, J = 8.4 Hz, 1H), 7.47−7.43 (m, 2H), 7.20−7.16 (m, 2H), 7.05 (dd, J = 6.8, 1.6 Hz, 1H), 5.93 (d, J = 5.8 Hz, 1H), 5.74 (d, J = 5.8 Hz, 1H), 5.41 (d, J = 5.8 Hz, 1H), 5.17 (d, J = 5.8 Hz, 1H), 2.28−2.23 (m, 1H), 2.11 (s, 3H), 0.88 (d, J = 6.90 Hz, 3H), 0.72 (d, J = 6.90 Hz, 3H); ^{13}C NMR (100 MHz, $CDCl_3$) δ 148.5, 141.1, 140.5, 128.0, 127.2, 123.4, 122.8, 121.5, 118.4, 115.9, 113.1, 102.3, 99.1, 89.5, 89.3, 82.4, 81.0, 30.7, 22.5, 21.7, 18.9; MS (ESI, MS) 429 (M − Cl)$^+$; HRMS (ESI) calcd for $C_{23}H_{23}N_2Ru$ m/z 429.0905, found m/z 429.0903. Anal. Calcd for **4a** ($C_{23}H_{23}ClN_2Ru$): C, 59.54; H, 5.00; N, 6.04. Found: C, 59.51; H, 5.02; N, 6.08.

Compound **4b** was synthesized using a procedure similar to that used for the synthesis of compound **4a**: yield 73%; light yellow solid; R_f = 0.26 (40% EtOAc/*n*-hexane); ^{1}H NMR (400 MHz, $CDCl_3$) δ 8.38 (s, 1H), 8.03 (s, 1H), 7.96 (d, J = 8.7 Hz, 1H), 7.66 (d, J = 8.4 Hz, 1H), 7.44−7.40 (m, 1H), 7.33 (d, J = 7.9 Hz, 1H), 7.19−7.16 (m, 1H), 6.86 (d, J = 7.8 Hz, 1H), 5.92 (d, J = 5.8 Hz, 1H), 5.73 (d, J = 5.8 Hz, 1H), 5.44 (d, J = 5.8 Hz, 1H), 5.16 (d, J = 5.8 Hz, 1H), 2.42 (s, 3H), 2.27−2.22 (m, 1H), 2.10 (s, 3H), 0.87 (d, J = 6.9 Hz, 3H), 0.72 (d, J = 6.9 Hz, 3H); ^{13}C NMR (100 MHz, $CDCl_3$) δ 148.4, 141.0, 128.9, 136.7, 130.1, 127.8, 121.4, 120.9, 118.0, 115.9, 112.7, 102.2, 98.9, 89.3, 82.7, 80.8, 30.7, 22.5, 21.7, 21.5, 19.0; MS (ESI, MS) 443 (M − Cl)$^+$; HRMS (ESI) calcd for $C_{24}H_{25}N_2Ru$ m/z 443.1061, found m/z 443.1090. Anal. Calcd for **4b** ($C_{24}H_{25}ClN_2Ru$): C, 60.31; H, 5.27; N, 5.86. Found: C, 60.33; H, 5.18; N, 5.84.

Compound **4c** was synthesized using a procedure similar to that used for the synthesis of compound **4a**: yield 75%; pale yellow solid; R_f = 0.27 (40% EtOAc/*n*-hexane); ^{1}H NMR (400 MHz, $CDCl_3$) δ 8.34 (s, 1H), 8.01 (s, 1H), 7.90 (d, J = 8.8 Hz, 1H), 7.62 (d, J = 8.4 Hz, 1H), 7.38 (d, J = 6.8 Hz, 1H), 7.36−7.32 (m, 1H), 7.14−7.10 (m, 1H), 6.89 (d, J = 8.0 Hz, 1H), 5.83 (d, J = 5.8 Hz, 1H), 5.69 (d, J = 5.8 Hz, 1H), 5.29 (d, J = 5.8 Hz, 1H), 5.09 (d, J = 5.8 Hz, 1H), 2.97−2.90 (m, 1H), 2.26−2.19 (m, 1H), 2.03 (s, 3H), 1.29−1.26 (m, 6H), 0.85 (d, J = 6.90 Hz, 3H), 0.68 (d, J = 6.90 Hz, 3H); ^{13}C NMR (100 MHz, $CDCl_3$) δ 147.4, 146. 138.2, 137.7, 127.4, 126.8, 121.6, 120.3, 116.9, 114.9, 111.7, 101.1, 98.4, 88.7, 88.0, 80.9, 79.9, 33.2, 29.7, 28.6, 23.6, 22.9, 21.5, 20.6; MS (ESI, MS) 471 (M − Cl)$^+$; HRMS (ESI) calcd for $C_{26}H_{29}N_2Ru$ m/z 471.1374, found m/z 471.1341. Anal. Calcd for **4c** ($C_{26}H_{29}ClN_2Ru$): C, 61.71; H, 5.78; N, 5.54. Found: C, 61.69; H, 5.58; N, 5.49.

Compound **4d** was synthesized using a procedure similar to that used for the synthesis of compound **4a**: yield 70%; pale green solid; R_f = 0.31 (40% EtOAc/*n*-hexane); ^{1}H NMR (400 MHz, $CDCl_3$) δ 8.38 (s, 2H), 7.87 (d, J = 8.92 Hz, 1H), 7.51 (d, J = 8.72 Hz, 1H), 7.41−7.39 (m, 1H), 7.31 (d, J = 8.2 Hz, 1H), 7.14−7.07 (m, 2H), 5.89 (d, J = 5.8 Hz, 1H), 5.68 (d, J = 5.8 Hz, 1H), 5.40 (d, J = 5.8 Hz, 1H), 5.15 (d, J = 5.8 Hz, 1H), 2.19−2.12 (m, 1H), 2.07 (s, 3H), 0.79 (d, J = 7.0 Hz, 3H), 0.64 (d, J = 7.0 Hz, 3H); ^{13}C NMR (100 MHz, $CDCl_3$) δ 164.4, 148.8, 136.8, 128.7, 123.2, 123.0, 121.9, 120.9, 119.7, 115.8, 112.7, 103.3, 99.6, 89.6, 89.4, 83.0, 81.0, 30.7, 22.5, 21.7, 19.0; MS (ESI, MS) 495 (M − Cl)$^+$; HRMS (ESI) calcd for $C_{24}H_{21}N_2ClF_3Ru$ m/z 531.0383, found m/z 531.0377. Anal. Calcd for **4d** ($C_{24}H_{22}ClF_3N_2Ru$): C, 54.19; H, 4.17; N, 5.27. Found: C, 54.19; H, 3.92; N, 5.18.

In a round-bottom flask equipped with a magnetic bar under a nitrogen atmosphere, 2-phenyl-2*H*-indazole **1a** (1 mmol) was dissolved in a freshly distilled dichloromethane solution (5 mL). Sodium acetate (1.2 mmol) was added to the flask at room temperature while its contents were being constantly stirred followed by the addition of $[(\eta^5\text{-}C_5Me_5)IrCl_2]_2$ **3** (0.5 mmol). The reaction mixture was stirred at room temperature for 20 h, and the progress of the reaction was monitored by TLC. After the complex had formed, dichloromethane was distilled under reduced pressure and diethyl ether (10 mL) was added to the mixture. The reaction mixture was stirred for 10 min to precipitate the product. The crystalline product was filtered through a fritted funnel and dried well. Orange-colored iridium complex **5a** was obtained in good yield (82%): R_f = 0.26 (40% EtOAc/*n*-hexane); ^{1}H NMR (400 MHz, $CDCl_3$) δ 8.37 (s, 1H), 7.89 (d, J = 7.2 Hz, 1H), 7.72−7.66 (m, 2H), 7.52 (d, J = 8.0 Hz, 1H), 7.36 (t, J = 7.6 Hz, 1H), 7.20−7.16 (m, 2H), 7.07 (dd, J = 8.0, 1.2 Hz, 1H), 1.76 (s, 15H); ^{13}C NMR (100 MHz, $CDCl_3$) δ 147.7, 146.9, 136.9, 128.4, 128.3, 122.9, 122.7, 121.6, 119.1, 115.2, 112.4, 88.5, 9.6; MS (ESI, MS) 521 (M − Cl)$^+$; HRMS (ESI) calcd for $C_{23}H_{25}ClIrN_2$ m/z 557.1336, found m/z 557.1349. Anal. Calcd for **5a** ($C_{23}H_{24}ClIrN_2$): C, 49.67; H, 4.35; N, 5.04. Found: C, 49.72; H, 4.26; N, 5.04.

Compound **5b** was synthesized using a procedure similar to that used for the synthesis of compound **5a**: yield 82%; yellow solid; R_f = 0.30 (40% EtOAc/*n*-hexane); ^{1}H NMR (400 MHz, $CDCl_3$) δ 8.37 (s, 1H), 7.89 (d, J = 7.5 Hz, 1H), 7.72−7.67 (m, 2H), 7.52 (d, J = 7.8 Hz, 1H), 7.37 (t, J = 6.84 Hz, 1H), 7.18 (s, 1H), 7.07 (dd, J = 7.4, 1.2 Hz, 1H), 1.77 (s, 15H) 1.55 (s, 3H); ^{13}C NMR (100 MHz, $CDCl_3$) δ 147.4, 146.4, 145.7, 136.8, 136.5, 134.1, 127.1, 122.7, 121.5, 120.5, 120.0, 117.6, 114.0, 111.1, 87.3, 20.4, 8.6; MS (ESI, MS) 535 (M − Cl)$^+$; HRMS (ESI) calcd for $C_{24}H_{26}IrN_2$ m/z 535.1719, found m/z 535.1699. Anal. Calcd for **5b** ($C_{24}H_{26}ClIrN_2$): C, 50.56; H, 4.60; N, 4.91. Found: C, 50.68; H, 4.58; N, 4.89.

Compound **5c** was synthesized using a procedure similar to that used for the synthesis of compound **5a**: yield 85%; pale yellow solid; R_f = 0.34 (40% EtOAc/*n*-hexane); ^{1}H NMR (400 MHz, $CDCl_3$) δ 8.69 (s, 1H), 7.72 (d, J = 7.2 Hz, 1H), 7.51 (d, J = 8.4 Hz, 2H), 7.29−7.27 (m, 2H), 7.19−7.15 (m, 1H), 7.05 (dd, J = 7.6, 1.2 Hz, 1H), 3.02−2.95 (m, 1H), 1.4 (s, 15H), 1.30 (d, J = 7.2 Hz, 6H); ^{13}C NMR (100 MHz, $CDCl_3$) δ 148.4, 147.5, 146.7, 140.3, 135.1, 128.1, 122.5, 121.5, 118.6, 115.1, 112.1, 88.4, 34.1, 24.7, 23.7, 9.6; MS (ESI, MS) 564 (M − Cl)$^+$; HRMS (ESI) calcd for $C_{26}H_{31}IrN_2$ m/z 564.2116, found m/z 564.2114. Anal. Calcd for **5c** ($C_{26}H_{30}ClIrN_2$): C, 52.20; H, 5.06; N, 4.68. Found: C, 52.26; H, 5.02; N, 4.42.

Compound **5d** was synthesized using a procedure similar to that used for the synthesis of compound **5a**: yield 80%; pale green solid; R_f = 0.29 (40% EtOAc/*n*-hexane); ^{1}H NMR (400 MHz, $CDCl_3$) δ 8.41 (s, 1H), 8.13 (s, 1H), 7.69 (t, J = 9 Hz, 2H), 7.55 (d, J = 8.3 Hz, 1H), 7.40 (t, J = 6.88 Hz, 1H), 7.31 (d, J = 8.44 Hz, 1H), 7.21 (t, J = 7.72 Hz, 1H), 1.77 (s, 15H); ^{13}C NMR (100 MHz, $CDCl_3$) δ 154.5, 148.0, 146.5, 144.6, 131.2, 129.5, 126.6, 120.7, 120.0, 118.4, 117.6, 112.6, 108.5, 86.4, 7.1; MS (EI, MS) 589 (M − Cl)$^+$; HRMS (ESI) calcd for $C_{24}H_{23}F_3IrN_2$ m/z 589.1437, found m/z 589.1425. Anal. Calcd for **5d** ($C_{24}H_{23}ClF_3IrN_2$): C, 46.19; H, 3.71; N, 4.49. Found: C, 46.23; H, 3.83; N, 4.69.

4.2. Biology. *4.2.1. General Methods.* MTT, dimethyl sulfoxide (DMSO), diphenylamine (DPA), 4% paraformaldehyde, glutaraldehyde, methanol, and Triton X-100 were purchased from Himedia (Mumbai, India). Cisplatin, DCFDA, and TRI Reagent were purchased from Sigma-Aldrich (Bangalore, India). Propidium iodide, JC-1 stain, DAPI, Hoechst 33342, the dead cell apoptosis kit with Annexin V FITC and PI for flow cytometry, CellEvent Caspase-3/7 Green ReadyProbes Reagent, and Alexa Fluoro 488 Phalloidin were purchased from ThermoFisher Scientific (Bangalore, India). The PrimeScript RT reagent Kit and SYBR Premix Ex Taq were purchased form DSS Takara Bio India Pvt. Ltd. (Bangalore, India). All of the primers were purchased from Eurofins (Bangalore, India). All of the compounds tested were freshly prepared and dissolved in DMSO. The final concentration of DMSO was maintained at 0.25% in all of the experiments.

4.2.2. Cell Culture and Reagents. Human MDA-MB-468 and MDA-MB-231 TNBC cells, human colon cancer cell line HCT-116, and human HEK 293 embryonic kidney cells were obtained from the National Center for Cell Sciences (NCCS, Pune, India). Cells were routinely maintained at 37 °C and 5% CO_2 in DMEM (Dulbecco's modified Eagle's medium, Himedia), complemented with 10% FBS (fetal bovine serum, Himedia), 100 IU/mL penicillin, and 100 μg/mL streptomycin (Himedia).

https://doi.org/10.1021/acs.inorgchem.1c02193
Inorg. Chem. 2021, 60, 17593−17607

4.2.3. Cell Viability Assay. The 3-(4,5-dimethylthiazol-2-yl)-2,5-diphenyltetrazolium bromide (MTT) (Himedia) assay was performed to check the cell viability as described previously.[14] In brief, MDA-MB-468, MDA-MB-231, HCT-116, and HEK 293 cell lines were seeded at a density of 1×10^4 cells/well in 96-well plates. Cells were exposed to different concentrations of **4a−d**, **5a−d**, and cisplatin for 48 h. After incubation, 25 μL of an MTT (5 mg/mL in 1× PBS) solution was added to each well and incubated for 4 h at 37 °C. The resulting formazan crystals were then solubilized with 100 μL of DMSO, and the color intensity of formazan was measured at 490 nm using a microplate reader (BioTek-ELx800). The results were compared with those of the untreated control, and each analysis point was assessed in triplicate. The cisplatin was used as a positive control, and DMSO was used as the vehicle control for cell viability inhibition.

4.2.4. Computational Details. Quantum chemical calculations were performed with the Gaussian software. All geometry optimizations were performed using the B3LYP functional with the LanL2 basis set. From these geometries, all reported data were obtained by means of vertical excitations using the same functional along with the more polarized def2-TZVPP basis set for all atoms except for iridium and ruthenium, for which the SDD basis set was used.

■ ASSOCIATED CONTENT

Supporting Information

The Supporting Information is available free of charge at https://pubs.acs.org/doi/10.1021/acs.inorgchem.1c02193.

Copies of ^{1}H NMR, ^{13}CNMR, and HRMS spectra of complexes **4a−d** and **5a−d**, absorption and fluorescence spectra of complexes in different solvents, stability study of complexes **4a−d** and **5a−d**, ESP maps of **4a**, **4c**, **4d**, **5a**, **5b**, and **5d**, ICP-MS analysis of complexes **4b** and **5c** in the MDA-MB-468 cell line and complexes **4b**, **5a**, **5b**, and **5d** that induced morphological changes in MDA-MB-468 cells after 24 h, single-crystal X-ray data of compound **5b**, and comparison of XRD- and DFT-derived structural details for **5b** (PDF)

Accession Codes

CCDC 2056445 contains the supplementary crystallographic data for this paper. These data can be obtained free of charge via www.ccdc.cam.ac.uk/data_request/cif, or by emailing data_request@ccdc.cam.ac.uk, or by contacting The Cambridge Crystallographic Data Centre, 12 Union Road, Cambridge CB2 1EZ, UK; fax: +44 1223 336033.

■ AUTHOR INFORMATION

Corresponding Author

Kaushik Chanda − *Department of Chemistry, School of Advanced Science, Vellore Institute of Technology, Vellore 632014, India;* orcid.org/0000-0002-7555-9322; Email: chandakaushik1@gmail.com

Authors

Rajeeva Lochana Panchangam − *Department of Biosciences, School of Biosciences and Technology, Vellore Institute of Technology, Vellore 632014, India*

Ramdas Nishanth Rao − *Department of Chemistry, School of Advanced Science, Vellore Institute of Technology, Vellore 632014, India*

Musuvathi Motilal Balamurali − *Chemistry Division, School of Advanced Sciences, Vellore Institute of Technology, Chennai 600127, India;* orcid.org/0000-0001-7948-9950

Tejashri B. Hingamire − *Biochemical Sciences Division, CSIR-National Chemical Laboratory, Pune 411008, India; Academy of Scientific and Innovative Research (AcSIR), Ghaziabad 201002, India*

Dhanasekaran Shanmugam − *Biochemical Sciences Division, CSIR-National Chemical Laboratory, Pune 411008, India; Academy of Scientific and Innovative Research (AcSIR), Ghaziabad 201002, India*

Venkatraman Manickam − *Department of Biosciences, School of Biosciences and Technology, Vellore Institute of Technology, Vellore 632014, India*

Complete contact information is available at: https://pubs.acs.org/10.1021/acs.inorgchem.1c02193

Notes

The authors declare no competing financial interest.

■ ACKNOWLEDGMENTS

The authors thank the Chancellor and Vice Chancellor of VIT for providing the opportunity to carry out this study. R.N.R., R.L.P., V.M., M.M.B., and K.C. thank the management of this university for providing seed money as a research grant. K.C. thanks ICMR, Government of India, for funding through Grant 45/03/2019-BIO/BMS. The authors also thank the Central Instrumentation Facility of VIT for recording the spectra and the Sophisticated Analytical Instrumentation Facility (SAIF), Gauhati University, for use of the single-crystal X-ray diffractometer.

■ REFERENCES

(1) Rosenberg, B.; VanCamp, L.; Trosko, J. E.; Mansour, V. H. Platinum compounds: a new class of potent antitumour agents. *Nature* **1969**, *222*, 385−386.

(2) Kelland, L. The resurgence of platinum-based cancer chemotherapy. *Nat. Rev. Cancer* **2007**, *7*, 573−584.

(3) (a) Raveendran, R.; Braude, J. P.; Wexselblatt, E.; Novohradsky, V.; Stuchlikova, O.; Brabec, V.; Gandin, V.; Gibson, D. Pt(iv) derivatives of cisplatin and oxaliplatin with phenylbutyrate axial ligands are potent cytotoxic agents that act by several mechanisms of action. *Chem. Sci.* **2016**, *7*, 2381−2391. (b) Petruzzella, E.; Sirota, R.; Solazzo, I.; Gandin, V.; Gibson, D. Triple action Pt(iv) derivatives of cisplatin: a new class of potent anticancer agents that overcome resistance. *Chem. Sci.* **2018**, *9*, 4299−4307.

(4) Thota, S.; Rodrigues, D. A.; Crans, D. C.; Barreiro, E. J. Ru(II) compounds: next-generation anticancer metallotherapeutics? *J. Med. Chem.* **2018**, *61*, 5805−5821.

(5) Licona, C.; Delhorme, J. B.; Riegel, G.; Vidimar, V.; Cerón-Camacho, R.; Boff, B.; Venkatasamy, A.; Tomasetto, C.; da Silva Figueiredo Celestino Gomes, P.; Rognan, D.; Freund, J. N.; Le Lagadec, R.; Pfeffer, M.; Gross, I.; Mellitzer, G.; Gaiddon, C. Anticancer activity of ruthenium and osmium cyclometalated compounds: identification of ABCB1 and EGFR as resistance mechanisms. *Inorg. Chem. Front.* **2020**, *7*, 678−688.

(6) Liu, Z.; Sadler, P. J. Organoiridium complexes: anticancer agents and catalysts. *Acc. Chem. Res.* **2014**, *47*, 1174−1185.

(7) Biancalana, L.; De Franco, M.; Ciancaleoni, G.; Zacchini, S.; Pampaloni, G.; Gandin, V.; Marchetti, F. Easily Available, Amphiphilic Diiron Cyclopentadienyl Complexes Exhibit in Vitro Anticancer Activity in 2D and 3D Human Cancer Cells through Redox Modulation Triggered by CO Release. *Chem. - Eur. J.* **2021**, *27*, 10169−10185.

(8) Yang, G.-J.; Wang, W.; Mok, S. W. F.; Wu, C.; Law, B. Y. K.; Miao, X.-M.; Wu, K.-J.; Zhong, H.-J.; Wong, C.-Y.; Wong, V. K. W.; Ma, D.-L.; Leung, C.-H. Selective inhibition of lysine-specific demethylase 5A (KDM5A) using a rhodium(III) complex for triple

negative breast cancer therapy. *Angew. Chem., Int. Ed.* **2018**, *57*, 13091−13095.
(9) Oun, R.; Moussa, Y. E.; Wheate, N. J. The side effects of platinum-based chemotherapy drugs: a review for chemists. *Dalton Trans.* **2018**, *47*, 6645−6653.
(10) Henry, N. L.; Shah, P. D.; Haider, I.; Free, P. E.; Jagsi, R.; Sabel, M. S. Chapter 88: Cancer of the Breast. In *Abeloff's Clinical Oncology*, 6th ed.; Niederhuber, J. E., Armitage, J. O., Doroshow, J. H., Kastan, M. B., Tepper, J. E., Eds.; Elsevier: Philadelphia, 2020.
(11) Lee, A.; Djamgoz, M. B. A. Triple Negative Breast Cancer: Emerging Therapeutic Modalities and Novel Combination Therapies. *Cancer Treat. Rev.* **2018**, *62*, 110−122.
(12) Badowska-kozakiewicz, A. M.; Budzik, M. P.; Liszcz, A.; Sobieraj, M. T.; Czerw, A. I.; Sobol, M.; Patera, J.; Deptała, A. Clinicopathological Factors Associated with Novel Prognostic Markers for Patients with Triple Negative Breast Cancer. *Arch. Med. Sci.* **2019**, *15*, 1433−1442.
(13) Pandy, J. G. P.; Balolong-garcia, J. C.; Cruz-ordinario, M. V. B.; Que, F. V. F. Triple Negative Breast Cancer and Platinum- Based Systemic Treatment : A Meta-Analysis and Systematic Review. *BMC Cancer* **2019**, *19*, 1065.
(14) Rademaker-Lakhai, J. M.; van den Bongard, D.; Pluim, D.; Beijnen, J. H.; Schellens, J. H. A phase I and pharmacological study with imidazolium-trans-DMSO-imidazole-tetrachlororuthenate, a novel ruthenium anticancer agent. *Clin. Cancer Res.* **2004**, *10*, 3717−3727.
(15) Clavel, C. M.; Paunescu, E.; Nowak-Sliwinska, P.; Griffioen, A. W.; Scopelliti, R.; Dyson, P. J. Modulating the Anticancer Activity of Ruthenium(II)-Arene Complexes. *J. Med. Chem.* **2015**, *58*, 3356−3365.
(16) Wilbuer, A.; Vlecken, D. H.; Schmitz, D. J.; Kraling, K.; Harms, K.; Bagowski, C. P.; Meggers, E. Iridium complex with antiangiogenic properties. *Angew. Chem., Int. Ed.* **2010**, *49*, 3839−3842.
(17) (a) He, L.; Tan, C. P.; Ye, R. R.; Zhao, Y. Z.; Liu, Y. H.; Zhao, Q.; Ji, L. N.; Mao, Z. W. Theranostic iridium(III) complexes as one- and two-photon phosphorescent trackers to monitor autophagic lysosomes. *Angew. Chem., Int. Ed.* **2014**, *53*, 12137−12141. (b) Nam, J. S.; Kang, M. G.; Kang, J.; Park, S. Y.; Lee, S. J. C.; Kim, H. T.; Seo, J. K.; Kwon, O. H.; Lim, M. H.; Rhee, H. W.; Kwon, T. H. Endoplasmic reticulum-localized iridium(III) complexes as efficient photodynamic therapy agents via protein modifications. *J. Am. Chem. Soc.* **2016**, *138*, 10968−10977. (c) Chen, M. H.; Wang, F. X.; Cao, J. J.; Tan, C. P.; Ji, L. N.; Mao, Z. W. Light-up mitophagy in live cells with dual-functional theranostic phosphorescent iridium(III) complexes. *ACS Appl. Mater. Interfaces* **2017**, *9*, 13304−13314. (d) Tian, Z.; Yang, Y.; Guo, L.; Zhong, G.; Li, J.; Liu, Z. Dual-functional cyclometalated iridium imine NHC complexes: highly potent anticancer and antimetastatic agents. *Inorg. Chem. Front.* **2018**, *5*, 3106−3112. (e) Li, J. J.; Guo, L.; Tian, Z.; Zhang, S.; Xu, Z.; Han, Y.; Li, R.; Li, Y.; Liu, Z. Half-Sandwich Iridium and Ruthenium Complexes: Effective Tracking in Cells and Anticancer Studies. *Inorg. Chem.* **2018**, *57*, 13552−13563. (f) Ma, W.; Zhang, S.; Tian, Z.; Xu, Z.; Zhang, Y.; Xia, X.; Chen, X.; Liu, Z. Potential anticancer agent for selective damage to mitochondria or lysosomes: Naphthalimide-modified fluorescent biomarker half-sandwich iridium (III) and ruthenium (II) complexes. *Eur. J. Med. Chem.* **2019**, *181*, 111599.
(18) (a) Kozieł, S. A.; Komarnicka, U. K.; Ziółkowska, A.; Skórska-Stania, A.; Pucelik, B.; Płotek, M.; Sebastian, V.; Bieńko, A.; Stochel, G.; Kyzioł, A. Anticancer potency of novel organometallic Ir(III) complexes with phosphine derivatives of fluoroquinolones encapsulated in polymeric micelles. *Inorg. Chem. Front.* **2020**, *7*, 3386−3401. (b) Kozieł, S. A.; Lesiów, M. K.; Wojtala, D.; Dyguda-Kazimierowicz, E.; Bieńko, D.; Komarnicka, U. K. Interaction between DNA, Albumin and Apo-Transferrin and Iridium(III) Complexes with Phosphines Derived from Fluoroquinolones as a Potent Anticancer Drug. *Pharmaceuticals* **2021**, *14*, 685.
(19) Wallace, D. C. Mitochondria and Cancer. *Nat. Rev. Cancer* **2012**, *12* (10), 685−698.
(20) Scatena, R. Mitochondria and Cancer: A Growing Role in Apoptosis, Cancer Cell Metabolism and Dedifferentiation. In *Advances in Mitochondrial Medicine. Advances in Experimental Medicine and Biology*, Vol. *942*; Scatena, R., Bottoni, P., Giardina, B., Eds.; Springer: Dordrecht, The Netherlands, 2012; pp 287−308.
(21) Martinou, J.-C.; Youle, R. J. Mitochondria in Apoptosis: Bcl-2 Family Members and Mitochondrial Dynamics. *Dev. Cell* **2011**, *21*, 92−101.
(22) Song, X. D.; Kong, X.; He, S. F.; Chen, J. X.; Sun, J.; Chen, B. B.; Zhao, J. W.; Mao, Z. W. Cyclometalated Iridium(III)-Guanidinium Complexes as Mitochondria-Targeted Anticancer Agents. *Eur. J. Med. Chem.* **2017**, *138*, 246−254.
(23) (a) Anthony, E. J.; Bolitho, E. M.; Bridgewater, H. E.; Carter, O. W. L.; Donnelly, J. M.; Imberti, C.; Lant, E. C.; Lermyte, F.; Needham, R. J.; Palau, M.; Sadler, P. J.; Shi, H.; Wang, F. X.; Zhang, W. Y.; Zhang, Z. Metallodrugs are unique: opportunities and challenges of discovery and development. *Chem. Sci.* **2020**, *11*, 12888−12917. (b) Tan, C. P.; Zhong, Y. M.; Ji, L. N.; Mao, Z. W. Phosphorescent metal complexes as theranostic anticancer agents: combining imaging and therapy in a single molecule. *Chem. Sci.* **2021**, *12*, 2357−2367.
(24) Panchangam, R. L.; Manickam, V.; Chanda, K. Assembly of Fully Substituted 2*H*-Indazoles Catalyzed by Cu_2O Rhombic Dodecahedra and Evaluation of Anticancer Activity. *ChemMedChem* **2019**, *14*, 262−271.
(25) De Angelis, M.; Stossi, F.; Carlson, K. A.; Katzenellenbogen, B. S.; Katzenellenbogen, J. A. Indazole Estrogens: Highly Selective Ligands for the Estrogen Receptor *β*. *J. Med. Chem.* **2005**, *48*, 1132−1144.
(26) Catalán, J.; del Valle, J. C.; Claramunt, R. M.; Boyer, G.; Laynez, J.; Gómez, J.; Jiménez, P.; Tomás, F.; Elguero, J. Acidity and Basicity of Indazole and its N-Methyl Derivatives in the Ground and in the Excited State. *J. Phys. Chem.* **1994**, *98*, 10606−10612.
(27) Tomassi, S.; Lategahn, J.; Engel, J.; Keul, M.; Tumbrink, H. L.; Ketzer, J.; Mühlenberg, T.; Baumann, M.; Schultz-Fademrecht, C.; Bauer, S.; Rauh, D. Indazole-Based Covalent Inhibitors To Target Drug-Resistant Epidermal Growth Factor Receptor. *J. Med. Chem.* **2017**, *60*, 2361−2372.
(28) Yellol, G. S.; Donaire, A.; Yellol, J. G.; Vasylyeva, V.; Janiak, C.; Ruiz, J. On the antitumor properties of novel cyclometalated benzimidazole Ru(ii), Ir(iii) and Rh(iii) complexes. *Chem. Commun.* **2013**, *49*, 11533−11535.
(29) Wang, F. X.; Chen, M. H.; Lin, Y. N.; Zhang, H.; Tan, C. P.; Ji, L. N.; Mao, Z. W. Dual Functions of Cyclometalated Iridium(III) Complexes: Anti-Metastasis and Lysosome-Damaged Photodynamic Therapy. *ACS Appl. Mater. Interfaces* **2017**, *9*, 42471−42481.
(30) Braselmann, H.; Michna, A.; Heß, J.; Unger, K. CFAssay : Statistical Analysis of the Colony Formation Assay. *Radiat. Oncol.* **2015**, *10*, 223.
(31) (a) Stras, S.; Holleran, T.; Howe, A.; Sofou, S. Interstitial Release of Cisplatin from Triggerable Liposomes Enhances Efficacy against Triple Negative Breast Cancer Solid Tumor Analogues. *Mol. Pharmaceutics* **2016**, *13*, 3224−3233. (b) Andey, T.; Sudhakar, G.; Marepally, S.; Patel, A.; Banerjee, R.; Singh, M. Lipid Nanocarriers of a Lipid-Conjugated Estrogenic Derivative Inhibit Tumor Growth and Enhance Cisplatin Activity against Triple-Negative Breast Cancer: Pharmacokinetic and Efficacy Evaluation. *Mol. Pharmaceutics* **2015**, *12*, 1105−1120.
(32) Circu, M. L.; Aw, T. Y. Reactive oxygen species, cellular redox systems, and apoptosis. Species, R. O.; Systems, C. R. NIH Public Access. *Free Radical Biol. Med.* **2010**, *48*, 749−762.
(33) Jeong, C.; Joo, S. H. Downregulation of Reactive Oxygen Species in Apoptosis. *J. Cancer. Preven.* **2016**, *21*, 13−20.
(34) Cao, J. J.; Zheng, Y.; Wu, X. W.; Tan, C. P.; Chen, M. H.; Wu, N.; Ji, L. N.; Mao, Z. W. Anticancer Cyclometalated Iridium(III) Complexes with Planar Ligands: Mitochondrial DNA Damage and Metabolism Disturbance. *J. Med. Chem.* **2019**, *62*, 3311−3322.
(35) Yang, B.; Chen, Y.; Shi, J. Reactive Oxygen Species (ROS)-Based Nanomedicine. *Chem. Rev.* **2019**, *119*, 4881−4985.

https://doi.org/10.1021/acs.inorgchem.1c02193
Inorg. Chem. 2021, 60, 17593−17607

(36) Lone, W. G.; Khan, M. S.; Raina, M. Etiology and Treatment Options of Triple Negative Breast Cancer (TNBC). *International Journal of Genetics and Cancer* **2014**, *1*, 5−12.
(37) Gohr, K.; Hamacher, A.; Engelke, L. H.; Kassack, M. U. Inhibition of PI3K/Akt/MTOR Overcomes Cisplatin Resistance in the Triple Negative Breast Cancer Cell Line HCC38. *BMC Cancer* **2017**, *17*, 711.
(38) Wang, F. X.; Chen, M. H.; Hu, X. Y.; Ye, R. R.; Tan, C. P.; Ji, L. N.; Mao, Z. W. Ester-Modified Cyclometalated Iridium(III) Complexes as Mitochondria-Targeting Anticancer Agents. *Sci. Rep.* **2016**, *6*, 21−23.
(39) Porporato, P. E.; Filigheddu, N.; Pedro, J. M. B. S.; Kroemer, G.; Galluzzi, L. Mitochondrial Metabolism and Cancer. *Cell Res.* **2018**, *28*, 265−280.
(40) Hearn, J. M.; Hughes, G. M.; Romero-Canelón, I.; Munro, A. F.; Rubio-Ruiz, B.; Liu, Z.; Carragher, N. O.; Sadler, P. J. Pharmaco-Genomic Investigations of Organo-Iridium Anticancer Complexes Reveal Novel Mechanism of Action. *Metallomics* **2018**, *10* (1), 93−107.
(41) Zhang, W. Y.; Du, F.; He, M.; Bai, L.; Gu, Y. Y.; Yang, L. L.; Liu, Y. J. Studies of Anticancer Activity in Vitro and in Vivo of Iridium(III) Polypyridyl Complexes-Loaded Liposomes as Drug Delivery System. *Eur. J. Med. Chem.* **2019**, *178*, 390−400.
(42) Cao, R.; Jia, J.; Ma, X.; Zhou, M.; Fei, H. Membrane Localized Iridium(III) Complex Induces Endoplasmic Reticulum Stress and Mitochondria-Mediated Apoptosis in Human Cancer Cells. *J. Med. Chem.* **2013**, *56* (9), 3636−3644.
(43) Liao, C.; Xu, D.; Liu, X.; Fang, Y.; Yi, J.; Li, X.; Guo, B. Iridium (III) Complex-Loaded Liposomes as a Drug Delivery System for Lung Cancer through Mitochondrial Dysfunction. *Int. J. Nanomed.* **2018**, *13*, 4417−4431.
(44) Tang, B.; Wan, D.; Wang, Y.-J.; Yi, Q.-Y.; Guo, B.-H.; Liu, Y.-J. An Iridium (III) Complex as Potent Anticancer Agent Induces Apoptosis and Autophagy in B16 Cells through Inhibition of the AKT/MTOR Pathway. *Eur. J. Med. Chem.* **2018**, *145*, 302−314.
(45) Sivandzade, F.; Bhalerao, A.; Cucullo, L. Analysis of the Mitochondrial Membrane Potential Using the Cationic JC-1 Dye as a Sensitive Fluorescent Probe. *Bio-Protoc.* **2019**, *9* (1−13), e3128.
(46) Walsh, J. G.; Cullen, S. P.; Sheridan, C.; Luthi, A. U.; Gerner, C.; Martin, S. J. Executioner Caspase-3 and Caspase-7 Are Functionally Distinct Proteases. *Proc. Natl. Acad. Sci. U. S. A.* **2008**, *105*, 12815−12819.
(47) Shi, Y. Caspase Activation, Inhibition, and Reactivation: A Mechanistic View. *Protein Sci.* **2004**, *13* (8), 1979−1987.
(48) DiPaiola, R. D. To arrest or not to G(2)-M Cell-cycle arrest: commentary re: Tyagi, A. K.; Singh, R. P.; Agarwal, C.; Chan, D. C. F.; Agarwal, R. Silibinin strongly synergizes human prostate carcinoma DU145 cells to doxorubicin-induced growth inhibition, G(2)-M arrest, and apoptosis. *Clin. Cancer Res.* **2002**, *8*, 3512−3519.

https://doi.org/10.1021/acs.inorgchem.1c02193
Inorg. Chem. 2021, 60, 17593−17607